



Supplementary Materials for

Systematic Analysis of Complex Genetic Interactions

Elena Kuzmin, Benjamin VanderSluis, Wen Wang, Guihong Tan, Raamesh Deshpande, Yiqun Chen, Matej Usaj, Attila Balint, Mojca Mattiazzi Usaj, Jolanda van Leeuwen, Elizabeth N. Koch, Carles Pons, Andrius J. Dagilis, Michael Prysizlak, Jason Zi Yang Wang, Julia Hanchard, Margot Riggi, Kaicong Xu, Hamed Heydari, Bryan-Joseph San Luis, Ermira Shuteriqi, Hongwei Zhu, Nydia Van Dyk, Sara Sharifpoor, Michael Costanzo, Robbie Loewith, Amy Caudy, Daniel Bolnick, Grant W. Brown, Brenda J. Andrews*, Charles Boone*, Chad L. Myers*

*correspondence to: chadm@umn.edu (C.L.M.), brenda.andrews@utoronto.ca (B.J.A.), charlie.boone@utoronto.ca (C.B.)

This PDF file includes:

Materials and Methods
Figs. S1 to S16
Tables S1 to S5
Additional Data Files Descriptions S1 to S7
References (64-82)

Materials and Methods

General information about the SGA dataset

In this study 182 double mutants and 364 corresponding single mutant control “query” strains were screened for genetic interactions against a diagnostic set of ~1,200 mutant “array” strains. Every double mutant query strain was screened alongside its two single mutant control strains, in two independent replicates, for a total of 1,092 screens. In total, we tested 410,399 double and 195,666 triple mutants for fitness defects and identified 9,363 negative digenic and 3,196 negative trigenic interactions. The raw genetic interaction data is available in Additional Data S1. The final trigenic interaction scores adjusted for digenic interactions are available in Additional Data S2, where we used an established interaction magnitude cut-off for digenic interactions ($p < 0.05$, $|\epsilon| > 0.08$) and trigenic interactions ($p < 0.05$, $\tau < -0.08$). The quality analysis of data produced at this threshold is provided in Fig. S5. The dataset can be browsed interactively and downloaded from

<http://boonelab.ccb.utoronto.ca/supplement/kuzmin2018/supplement.html>

Data files S1 to S7 were also deposited in the DRYAD Digital Repository (doi:10.5061/dryad.tt367).

SGA query strain construction

Strain maintenance

All query strains were maintained on YEPD media (1% yeast extract, 2% peptone, 2% glucose, 0.012% adenine) supplemented with 100 µg/mL nourseothricin (Werner Bioagents) and array strains on YEPD supplemented with 200 µg/mL geneticin (Agri-Bio). Array strains were obtained either from non-essential gene deletion collection (13) or a collection of temperature-sensitive alleles of essential genes (64).

Query strain construction

Double mutant query strains were constructed by crossing *gene-1* and *gene-2* single mutant strains and isolating haploid meiotic progeny of the desired genotype (Additional Data S3).

Single mutant (*gene-1*) transformation for downstream haploid selection:

Single mutants for *gene-1* strains were (*MAT α gene-1::natMX4 can1 Δ ::STE2pr-Sp_his5 lyp1 Δ his3 Δ 1 leu2 Δ 0 ura3 Δ 0 met15 Δ 0*) were constructed previously (15) and transformed with plasmid p6981, which was used for the downstream *MAT α* haploid selection.

Single mutant (*gene-2*) construction by marker switching:

Single mutants for *gene-2* strains were obtained from the yeast deletion collection (*MAT α gene-2 Δ ::kanMX4 his3 Δ 1 leu2 Δ 0 ura3 Δ 0 met15 Δ 0*) or our previously constructed collection of temperature sensitive alleles of essential genes (64) and marker switched from *kanMX4* to *KIURA3* by PCR-mediated gene deletion strategy using high efficiency LiAc transformation (65, 66). The primer sequences that were used to amplify the *KIURA3* cassette contained 55 bp homology to 5' of the *kanMX4* cassette (5'-3': ACATGGAGGCCCAAGAATACCCTCCTTGACAGTCTTGACGTGCGCAGCTCAGG GGCcggagacaatcatatgggag) and 55 bp homology to 3' of the *kanMX4* cassette (5'-3':

CAGTATAGCGACCAGCATTCACATACGATTGACGCATGATATTACTTTCTGCG
CAAtctggaggaagtttgagagg).

A second strategy was also used for marker switching *gene-2* strains from *kanMX4* to *KIURA3*. To marker switch *gene-2*, strains were transformed with p7011, which contains *KIURA3* ORF excluding the start codon, flanked at the 5' end by 147 bp of the 5' *kanMX4* ORF excluding the start codon, and flanked at the 3' end by 198 bp of the 5' TEF terminator, such that upon a transformation into a strain with a *yfgΔ::kanMX4* allele the *KIURA3* will recombine by homologous recombination immediately after the start codon of *kanMX4*, enabling selection for Ura⁺ colonies. In this way, *yfgΔ::kanMX4* will be marker switched to *yfgΔ::KIURA3*. The transformants were recovered in liquid SD-Ura overnight, and then the transformation mixture was spotted on SD-Ura plates and incubated for additional 2 days. The resultant transformation spots were scraped, resuspended in 200 μl water, plated on SD-ura plates and incubated for 2-7 days. Replica plating on SD-ura and YEPD+G418 enabled the identification of Ura⁺ and kanR colonies. Further replica plating on YEPGalactose induced expression of the toxic *GAL1pr-KAR1* on the plasmid, which enables selection of clones that lost the plasmid.

The integrated *KIURA3* cassette can be amplified using the following set of primers (5'-3'): Forward - ACATGGAGGCCCAAGAATACC and Reverse – CAGTATAGCGACCAGCATTC that anneal to *TEF* promoter and *TEF* terminator, respectively. Y8835 (*MATα can1Δ::STE2pr-Sp-his5 lyp1Δ ura3Δ0::natMX4 leu2Δ0 his3Δ1 met15Δ0*) was used to construct Y13096 by PCR-mediated deletion of *HO* using *KIURA3* from p5749 with the following primers (5'-3'): Forward (45 bp homology to *YDL22C* locus and 20 bp to *KIURA3* promoter) – CATATCCTCATAAGCAGCAATCAATTCTATCTATACTTTAAAATGcggagacaatcatatgggag and Reverse - (45 bp homology to *YDL22C* locus and 20 bp to *KIURA3* terminator) – TTACTTTTATTACATACAACCTTTTAACTAATATACACATTTTAtctggaggaagtttgagagg. For upstream confirmation of *KIURA3* integration, the forward primer was designed such that it would anneal around 400 bp upstream of the marker cassette integration site and the reverse primer was internal to the *KIURA3* ORF (5'-3') GTGACCTCTTGCGCACCTTG and for downstream confirmation of *KIURA3* integration, the forward primer was designed such that it would be internal to the *KIURA3* ORF (5'-3') CAAGGTGCGCAAGAGGTCAC and the reverse primer would anneal around 400 bp downstream of the marker cassette integration site.

Double mutant query strain construction by crossing single mutants *gene-1* & *gene-2*:

The resulting *gene-1* and *gene-2* strains were crossed, sporulated and *MATα* meiotic progeny were selectively germinated using plasmid-based *STE3pr-hphR* marker contained in p6981, and induction of *GAL1pr-KAR1*, which is on the same plasmid enabled counter selection for query strains lacking the plasmid. Final double mutant strains were of the following genotype: *MATα gene-1::natMX4 gene-2::KIURA3 can1Δ::STE2pr-Sp_his5 lyp1Δ his3Δ1 leu2Δ0 ura3Δ0 met15Δ0*. Single mutant control query strains were constructed equivalently, such that each strain carried a mutation of one member of the gene pair and the marker of the second mutation in the benign *hoΔ*

locus. p4339 and p5749 were used to amplify *natMX4* and *KIURA3*, respectively. PCR for marker amplification was carried out as described previously (67).

Synthetic genetic array analysis for trigenic and digenic interactions

Query fitness estimation

A high-density array was assembled to estimate query strain fitness. The strains on the array were arranged such that those carrying mutations in genes that are on the same chromosome were maximally separated. The gaps on the array (including the border rows and columns) were filled with either Y13096 (*MATa ura3Δ::natMX4 hoΔ::KIURA3 can1Δ::STE2pr-Sp_his5 lyp1Δ his3Δ1 leu2Δ0 ura3Δ0 met15Δ0 LYS2+*) or Y14412 (*MATa his3Δ1::natMX4 hoΔ::KIURA3 can1Δ::STE2pr-Sp_his5 lyp1Δ his3Δ1 leu2Δ0 ura3Δ0 met15Δ0 LYS2+*), which enabled the arrays to be crossed to two different control strains, each carrying a marked deletion in a benign locus, (*his3* and *ura3*): DMA1 (*MATa his3Δ1::kanMX4 leu2Δ0 ura3Δ0 met15Δ0*) and Y14420 (*MATa his3Δ1 leu2Δ0 ura3Δ0::kanMX4 met15Δ0*). This minimized the amount of missing data caused by genes of interest being linked genetically to *HIS3* or *URA3* genomic loci. Mutants with both query genes residing in *HIS3* or *URA3* linkage groups were assigned a fitness value of NaN. Once the arrays were crossed to the aforementioned strains, they were subjected to SGA, as described below, and scored for colony size in order to estimate fitness (Fig. S1, Additional Data S4). The quantitative scoring method employed for single and double mutant fitness estimation was described previously (8), with the exception that bootstrapped means, instead of medians, across replicates were used in variance estimation and final fitness values. Each high-density array was screened in triplicate for a total of 6 replicates. Since the arrays were in 1536-colony format, there are 4 technical replicates of mutants on the array resulting in a total of between 12 and 24 colony measurements for each fitness estimate. To control for differences associated with the choice of the control strain (*his3Δ1* or *ura3Δ0*) we fit a first-order polynomial, which was then applied to adjust the values for all *ura3Δ0::kanMX4* strains. After the adjustment, double mutant fitness estimates from the two assays were averaged together, and the resulting standard can be found in Additional Data S4. Fitness estimates were compared to another SGA dataset (7) and any mutants with $|\text{difference}| > 0.2$ were set to NaN. During the genetic interaction scoring process all NaN fitness estimates were assigned a value of 1.0, as described previously (8).

Array fitness estimation

Estimates of the mean single mutant fitness of each array strain were taken from a previous study (7). Estimates of the variance of array single mutant fitness used in the calculation of interaction p-values, were obtained by screening a wild-type control query strain, Y13096, against the diagnostic array ($n = 91$).

Negligible effect of *HO* deletion

To assess whether the deletion of *HO* affected strain fitness, genome-wide screens were conducted using control query strain Y13096 ($n = 7$) and compared to those performed using Y8835 ($n = 71$) (7), resulting in *ura3Δ::naMX4 hoΔ::KIURA3 gene-xΔ::kanMX4* mutants vs. *ura3Δ::naMX4 gene-xΔ::kanMX4* mutants, respectively.

Pearson correlation coefficient of 0.97, with $r^2 = 0.94$ showed a negligible role of the deletion of *HO* on strain fitness (Fig. S2).

Triple mutant synthetic genetic array (SGA) analysis

Several selection strategies were tested to optimize the experimental set-up and prevent a large variation in colony size. In a standard SGA experiment, each query gene is selected sequentially and so we first extended this approach to triple mutant selection by pinning to medium that first selected for one single query gene, followed by double and triple mutant query gene progeny: $\text{kanR} \rightarrow \text{Ura}^+/\text{kanR} \rightarrow \text{Ura}^+/\text{kanR}/\text{natR}$, which reduces the number of progeny by 2-fold with each successive selection. We then tested the efficacy of triple mutant selection when one of the selection steps was eliminated. Single mutant selection followed by direct selection for triple mutants ($\text{kanR} \rightarrow \text{Ura}^+/\text{kanR}/\text{natR}$) reduced the progeny first by 2-fold then by 4-fold, which produced uneven colonies that were difficult to score. However, selecting first for double, then triple mutants ($\text{Ura}^+/\text{kanR} \rightarrow \text{Ura}^+/\text{kanR}/\text{natR}$), reduced the progeny first by 4-fold and then by 2-fold, producing round and even colonies that were easily scored. The first and the third approaches showed a high Pearson correlation coefficient of normalized colony sizes ($r = 0.84$) and no significant difference for binned colony size variability (t test, $p = 0.66$). Thus, the third approach ($\text{Ura}^+/\text{kanR} \rightarrow \text{Ura}^+/\text{kanR}/\text{natR}$) was used for all triple mutant screens which eliminated one selection step thereby proving to be more time and cost effective.

Thus, SGA analysis was conducted as described previously (67) with modifications (Fig. 1B). Briefly, lawns of query mutant strains were grown at 26°C for 2 days and then pinned onto fresh YEPD plates. The diagnostic mutant array was then pinned on top of the query strain. The mated mix was incubated at room temperature for a day and then diploids were selected by pinning the resulting *MATa/a* diploid zygotes to YEPD + G418/clonNAT and incubating at 26°C for 2 days. The resulting $\text{natR}/\text{Ura}^+/\text{kanR}$ *MATa/a* diploids were sporulated by pinning onto enriched sporulation agar plates and incubating at 22°C for 7 days. To select for *MATa* meiotic haploid progeny, spores were pinned onto SD – His/Arg/Lys + canavanine/thialysine (50 µg/ml of each analog) and incubated at 26°C, 2 days. Following haploid selection, the resulting colonies were pinned onto SD_{MSG} – His/Arg/Lys/Ura + canavanine/thialysine/G418 (0.17% yeast nitrogen base without amino acids and ammonium sulfate, 0.1% monosodium glutamic acid, 0.2% amino acid supplement, 2% agar, 2% glucose, 50 µg/mL of each analog, for antibiotic concentration see ‘Strain Maintenance’ section), after which $\text{Ura}^+/\text{kanR}/\text{natR}$ *MATa* meiotic haploid progeny were selected by pinning the double/triple mutant haploid mix onto SD_{MSG} – His/Arg/Lys/Ura + canavanine/thialysine/G418/clonNAT to select for final triple mutants. The incubation temperature for all the selection steps was 26°C, except for sporulation, which was conducted at 22°C. Every double mutant query strain was screened alongside its two single mutant control strains in two independent replicates. Because trigenic interactions were derived by profile subtraction (see section on ‘Quantifying trigenic interactions’ below), single mutant control queries and their corresponding double mutant control query were screened in the same batch to minimize the compounding of systematic effects.

Diagnostic array construction

COMPRESS-GI (COMpress Profiles Related to Epistasis by Selecting Informative Genes), a diagnostic gene set selection algorithm, was employed to select mutants for construction of the diagnostic array that was functionally representative of the entire genome (Fig. S3A) (17). The process was based on genetic interaction profiles gathered from screens against arrays consisting of nonessential gene deletion mutants (NES) and temperature sensitive alleles of essential genes (ES) from (15). The digenic interactions associated with the selected subset of array mutant strains were sufficient to recapitulate functional profiles seen in our reference genetic interaction network (15) (Fig. S3B-C) since the genetic interaction profiles of queries based on this subset of array strains produced query-query genetic interaction profile similarity scores ranked similarly to query-query genetic interaction profile similarity scores based on the genome-wide set of array strains (Fig. S3B-C). Precision and recall were calculated as previously described (68). True positive pairs were represented by query pairs that were co-annotated to the same GO biological process term and ranked at the top of the list for query-query profile similarity scores. In fact, the algorithm reached a maximal area under the precision-recall curve using ~ 200 strains and to maximize the detailed biological information for each screen while maintaining experimental feasibility, we iterated six times selecting different array strains with each iteration, while holding out array strains that were selected in previous iterations. A total of 1,182 mutants (990 NES, 192 ES) were selected (Additional Data S5) that provide a representative view of the global digenic interaction network (Fig. S3B-C). Some array mutants were removed for quality control reasons. Each essential gene on the diagnostic array was represented by a single temperature sensitive allele. Pilot screens involving 12 query mutant strains were conducted against the whole genome array and the diagnostic array (data available upon request). Mutant strains on the diagnostic array cover all major biological processes in the cell (Fig. S3D) and captured a range of single mutant fitness estimates and genetic interaction degrees comparable to those on the whole genome array (Fig. S3E-F).

Summary of quantitative fitness-based model of genetic interactions

Digenic interactions were scored as previously described (8) and trigenic interactions were scored using the following models:

$$\begin{aligned}(\text{digenic}) \varepsilon_{i,j} &= f_{ij} - (f_i f_j) \\(\text{trigenic}) \tau_{i,j,k} &= f_{ijk} - f_i f_j f_k - \varepsilon_{j,k} f_i - \varepsilon_{i,k} f_j - \varepsilon_{i,j} f_k\end{aligned}$$

where ε is the digenic interaction score, τ is the final adjusted trigenic interaction score, f is fitness and i, j , and k are individual mutations.

The final adjusted trigenic interaction profile consists only of trigenic interaction scores that have been corrected for any digenic interactions. These final corrected scores are denoted as ‘adjusted trigenic interaction scores’ in Additional Data S2.

Quantifying trigenic interactions

Derivation of the quantitative fitness-based model for trigenic interactions

The trigenic model quantifies differences in a similar manner as the digenic interaction model (Fig. 1C). The digenic interaction score under the multiplicative model is

$$\varepsilon_{i,j} = f_{ij} - (f_i f_j)$$

where ε is the digenic interaction score, f_{ij} is the observed fitness of the double mutant and $f_i f_j$ is the expected fitness based on the product of single mutant fitness estimates. The expected fitness of a triple mutant is likewise the product of the single mutant fitness estimates $f_{ijk \text{ expected}} = f_i f_j f_k$, however, this assumes independence and if two of the three mutants (say i and j) have a digenic interaction, then we must account for it. In this case, the expected fitness would be the product of the interacting double mutant and the unrelated single mutant $f_{ijk \text{ expected}} = f_{ij} f_k$. Expressing this equation in terms of single mutant fitness terms only provides the following:

$$f_{ijk \text{ expected}} = (f_i f_j + \varepsilon_{i,j}) f_k$$

It then becomes evident that the expectation contains digenic interaction effects that are scaled by the fitness of non-interacting genes. As a result, a trigenic interaction score would be:

$$\tau_{i,j,k} = \text{observed} - \text{expected} = f_{ijk} - (f_i f_j + \varepsilon_{i,j}) f_k$$

By accounting for the remaining two possible digenic interactions and after rearranging the terms for clarity, the expression for trigenic interactions becomes:

$$\tau_{i,j,k} = f_{ijk} - f_i f_j f_k - \varepsilon_{j,k} f_i - \varepsilon_{i,k} f_j - \varepsilon_{i,j} f_k$$

Furthermore, it would be desirable for the expression to contain terms such that they are either single mutant fitness estimates or genetic interaction scores obtained from the available single, double and triple mutant screens. For example, if we screen the double mutant ij as a query, we can measure interactions between the double mutant ij and an array gene (k):

$$\varepsilon_{ij,k} = f_{ijk} - f_i f_j f_k$$

By solving the latter two equations for f_{ijk} and setting them equal to each other, we can solve for the trigenic interaction term from known quantities:

$$\tau_{i,j,k} = \varepsilon_{ij,k} - \varepsilon_{i,k} f_j - \varepsilon_{j,k} f_i$$

Where $\tau_{i,j,k}$ is the trigenic interaction score after accounting for single and double mutant effects, $\varepsilon_{ij,k}$ is the genetic interaction score measured between the double mutant query and an array k , $\varepsilon_{i,k}$ and $\varepsilon_{j,k}$ are genetic interaction scores obtained from accompanying single mutant control screens, and f_i and f_j are single mutant fitness estimates available from a previous study (7).

Comparison with MinDC model

The resulting final equation for triple mutant SGA is similar to a previously described MinDC model (18), but differs in two aspects (Fig. S4A).

$$\text{Residual}_{(\text{MinDC})-(\tau\text{-SGA})} = (\varepsilon_{1,2} - \varepsilon_2) - (\varepsilon_{1,2} - f_1 \varepsilon_2 - f_2 \varepsilon_1) = \varepsilon_2 (f_1 - 1) + f_2 \varepsilon_1$$

Firstly, it recognizes that as a consequence of an additive model of epistasis, digenic interactions must be scaled by the single mutant fitness of the third gene to account for their expected magnitude in a different genetic background. In practice, most genes have negligible single mutant effects and these adjustments tend to be minor. More importantly, the τ -SGA model accounts for digenic contributions from all constituent pairs, not only the more extreme. We reassessed our data under the MinDC model and found that while the majority of negative trigenic interactions achieve a significant score under either model (using a threshold of ≤ -0.08 for both), there are differences (Fig. S4B). Specifically, in some cases where both control screens show a negative epsilon,

and the MinDC score accounts for only the more extreme of the two, the MinDC model reports interactions which despite their large magnitude can be accounted for by the sum of digenic effects (Fig S4C, right panel). Similarly, in cases where one or both of the control screens show a positive epsilon, and again one is ignored by MinDC, τ -SGA can recover interactions where the triple mutant deviates from expectation (Fig. S4C, left panel).

Evaluation of reproducibility of genetic interactions

Each trigenic score is influenced by several observations: three single mutant fitness estimates, digenic interactions between three possible pairs, and the additional triple mutant effect on fitness. To confidently identify trigenic interactions, we need to ensure that the triple mutant effect was not a false positive and similarly that digenic interaction screens did not produce false negatives, either of which would produce a false positive trigenic interaction (refer to Fig. S5A-E). To address these issues, consider that interactions discovered in each triple mutant screen (before the quantitative adjustment for digenic interactions) would include: *a*) real trigenic interactions; *b*) real digenic interactions that were true positives in the control double mutant screens; *c*) real digenic interactions that were false negatives in the control double mutant screens; *d*) false positives. To calculate each of these parameters, we reasoned that the number of true trigenic interactions (*a*) depends on the number of observed trigenic interactions (*T*) and the recall of a screen (*R*), while the number of real digenic interactions that were detected in triple mutant screens and were true positives in the control double mutant screens relates to R^2 . The number of real digenic interactions that were detected in triple mutant screens but were missed in the control double mutant screens depends on the number of the observed digenic interactions (*D*) and recall (*R*).

$$(Real\ trigenic\ interactions)\ a = R \times T$$

$$(Real\ digenic\ interactions, observed\ in\ controls)\ b = R^2 \times D$$

$$(Real\ digenic\ interactions, missed\ in\ controls)\ c = R \times D \times (1 - R)$$

$$(False\ positives)\ d = (a + b + c) \times \frac{(1 - P)}{P}$$

Since *a*, *b*, *c* encompass real genetic interactions then technical precision of a screen can be expressed as:

$$(Technical\ screen\ precision)\ (P) = \frac{(a + b + c)}{(a + b + c + d)}$$

After removing digenic interactions that were observed in double mutant screens, the precision of a trigenic interaction screen is:

$$(Trigenic\ interaction\ precision) = \frac{a}{(a + c + d)}$$

Assuming that the number of trigenic interactions is on the same order as the number of digenic interactions then we can use the equations above to solve for trigenic interaction precision in terms of precision and recall for digenic screens of individual mutants.

$$(Trigenic\ interaction\ precision) = \frac{P}{P(2 - R) + 2(1 - P)}$$

The screen noise was similar for double mutants (Fig. S5B left) compared to raw triple mutant scores (Fig. S5B middle) with the correlation between independent replicates of 0.9-0.91. However, the adjusted trigenic interaction scores showed more variability with the correlation coefficient between replicates decreasing to 0.74-0.81 (Fig. S5B right). Given that the final trigenic interaction score is generated from the subtraction of several terms, this reduction is expected and to mitigate this effect, we conducted every screen in duplicate (Fig. S5C).

Empirical estimates of technical precision and recall of SGA screens are affected by the number of replicates (Fig. S5C). Single replicate precision and recall of a digenic interaction screen of ~50% and ~40%, respectively, resulted in an estimated 28% precision for identifying trigenic interactions. However, performing screens in multiple replicates increased precision at little cost to recall. As such, conducting two replicates results in precision and recall of a digenic interaction screen of 80% and 38%, respectively, elevating trigenic screen precision to ~50%, similar to the precision achieved with one digenic interaction screen replicate reported in another large-scale SGA study (15).

Control digenic interaction screens ($n = 20$) with 4 replicates were also used to evaluate reproducibility of genetic interactions (Fig. S5D). They were combined in random pairing of 2 replicates and scored. For each combination of datasets, we calculated the overlap fold enrichment as the ratio between the fraction of significant negative interaction pairs ($p < 0.05$) at varying score thresholds in the first dataset with an interaction in the second and the fraction of non-interacting pairs in the first dataset with an interaction in the second. The average fold enrichment for overlapping significant negative genetic interactions averaged across 3 combinations of data sets showed that interactions with stronger magnitude are more likely to be detected in both replicates. This is consistent with the observation that the distribution of digenic interactions that are detected and undetected in raw unadjusted triple mutant screens tend to be skewed to the right, with the interactions characterized by weaker magnitudes less likely to be detected (Fig. S5E). Since, conducting two replicates improves precision at little cost to recall and reproducibility of interactions in two random screens mirrors the reproducibility of digenic interactions that are detected in raw triple mutant screens, all trigenic interaction screens were performed twice.

Validation of trigenic interactions

Tetrad analysis and random spore analysis were used to confirm negative genetic interactions using standard techniques. Briefly, for tetrad analysis a double mutant query strain was crossed to single mutant array strains of interest, sporulated and 20-24 tetrads were dissected on SD complete medium and incubated at 30°C for 2-3 days for deletion mutants and an additional 22°C incubation step was included for temperature sensitive mutants. Replica plating on YEPD + clonNAT (100 µg/mL) identified natR meiotic progeny that carry the query mutation of gene 1, growth on SD-Ura identified ura⁺ spores that carry the query mutation of gene 2, and growth on YEPD+G418 (200 µg/ml) identified kanR spores that carry the array mutation; standard mating type assays were also included.

Trigenic interactions were validated using a set of manually confirmed synthetic sick or lethal interactions from a previously reported screen using a *cln1Δ cln2Δ* double

mutant query strain (19) whereby 19 of 36 genes were common to both studies. We retested these interactions by tetrad analysis to obtain a high confidence set of 15 interactions that were confirmed as synthetic sick or lethal trigenic interactions, 2 interactions did not confirm and another 2 were inconclusive. Thus, the analysis was restricted to 15 interactions of which 9 showed a significant negative trigenic interaction in our SGA screen at an intermediate cut-off, $\tau \leq -0.08$, resulting in a true positive rate of ~60% and a false negative rate of ~40% (see Table S2, Fig. S6A), consistent with another high-throughput SGA study (15). The difference could be attributed to the reproducibility or magnitude of the genetic interaction in addition to the genotype of the background strain used in the two studies.

Random spore analysis was performed as described previously (69) with additional steps for the selection of triple mutants. A small amount of spores (~ the size of a pinprick) was resuspended in 1 ml of sterile water and mixed well. Then, 20 μ l of the suspension was plated on SD – His/Arg/Lys + canavanine/thialysine; 40 μ l on SD_{MSG} – His/Arg/Lys + canavanine/thialysine/G418; 40 μ l on SD_{MSG} – His/Arg/Lys + canavanine/thialysine/clonNAT; 40 μ l on SD_{MSG} – His/Arg/Lys/Ura + canavanine/thialysine; 80 μ l on SD_{MSG} – His/Arg/Lys/Ura + canavanine/thialysine/G418, 80 μ l on SD_{MSG} – His/Arg/Lys/Ura + canavanine/thialysine/clonNAT, 80 μ l on SD_{MSG} – His/Arg/Lys + canavanine/thialysine/G418/clonNAT, and 160 μ l on SD_{MSG} – His/Arg/Lys/Ura + canavanine/thialysine/G418/clonNAT. The plates were incubated at RT for 4 days and scored by comparing growth on the single, double, and triple drug selection plates.

Screening a *cln1 Δ cln2 Δ* query mutant against the diagnostic array identified 73 negative trigenic interactions at an intermediate cut-off, $\tau \leq -0.08$, $p < 0.05$. An arbitrary set was selected for confirmations by random spore analysis and 26 of 34 negative trigenic interactions were confirmed, generating a true positive rate of 76% and false positive rate of 24% (see Table S2, Fig. S6B).

Representative digenic interactions of *MDY2* and *MTC1* single mutant queries as well as representative trigenic interactions of *MDY2-MTC1* double mutant query were confirmed by tetrad analysis as described above and are reported in Additional Data S6, with sample tetrad analysis images reported in Fig. S9A.

Classifying trigenic interactions into novel vs. modified

Our model for trigenic interactions allows for a trigenic interaction involving two genes connected by a digenic interaction, providing the triple mutant demonstrates a significant deviation from the expected fitness of the double mutant when combined with the third perturbation. We term cases where such an overlap exists as “modified” trigenic interactions because the third perturbation exacerbates or alleviates a previously known digenic interaction leading to a more extreme phenotype than expected, and thus can be said to modify an existing interaction. Alternatively, we observe a “novel” trigenic interaction in cases where none of the two gene-gene connections within the triad overlaps with a previously known digenic interaction. In these cases, we have gained novel functional information for genes that were not previously observed to interact in digenic space. In practice, a trigenic interaction (τ_{ijk}) between a double mutant query (Q_{ij}) and an array (A_k) is called novel if there is no significant interaction between either single mutant control query (Q_i or Q_j) and the array (A_k), and also no interaction between query

gene pair itself. Digenic interactions between Q_i-A_k or Q_j-A_k were measured using our single mutant control queries. Query pair interactions (Q_i-Q_j) were measured using the single and double mutant fitness standard (Additional Data S4) and applying the multiplicative model to derive the genetic interaction between the two query genes. Each query mutant fitness score has an associated standard deviation, and these were combined to calculate the expected variance of the double mutant fitness under the product. As epsilon scores are approximately normally distributed, this expected variance can be used to calculate a p-value. If any such digenic interaction exists, either positive or negative, the trigenic interaction is called modified (Fig. S8A). We classified negative trigenic interactions into 1,859 modified and 1,024 novel at the following thresholds for digenic interactions ($p < 0.05$, $|\epsilon| > 0.08$) and trigenic interactions ($p < 0.05$, $\tau < -0.08$). A further 313 trigenic interactions have no overlapping digenic interaction but stem from double mutant queries for which double mutant fitness estimates have not been generated in our standard due to quality control and have corresponding NaN values. Due to this uncertainty, these interactions have been withheld from the novel class in Fig. S8A-C. Furthermore, 1,508 modified trigenic interactions overlap a significant negative digenic interaction, 243 modified trigenic interactions overlap a significant positive digenic interaction, and 108 modified trigenic interactions overlap both significant positive and negative digenic interactions (Fig. S8A, Additional Data S2). To simplify the analysis depicted in Fig. S8B and due to the relatively small class size of 8 modified trigenic interactions that overlapped a query-query interaction and two digenic interactions (one positive and one negative) involving query-array pair, this group was collapsed with two other groups and half of these interactions were summed with (1) a class containing modified trigenic interactions that overlapped a query-query interaction and a positive query-array interaction, and half were summed with (2) a class containing modified trigenic interactions that overlapped a query-query interaction and a negative query-array interaction. The same was applied to 17 modified trigenic interactions that overlapped two digenic interactions (one positive and one negative) involving query-array pair but did not show a query-query interaction. This group was collapsed with two other groups and half of these interactions were summed with a class containing modified trigenic interactions that overlapped a positive query-array interaction and half were summed with a class containing modified trigenic interactions that overlapped a negative query-array interaction.

Analysis of functional relatedness of digenic and trigenic interactions

Frequency of negative genetic interactions within and between biological processes was calculated using the fraction of screened query-array combinations exhibiting negative interactions belonging to functional gene sets annotated by SAFE on the global genetic interaction network (55). For each biological process the fold-increase over the background fraction of interactions (digenic = 0.023, trigenic = 0.016) was calculated and significance was assessed using a hypergeometric test; Benjamini-Hochberg method was used to correct for multiple comparisons. The “within process” category received a count for any combinations in which both genes for digenic interactions or all three genes for trigenic interactions, were annotated to the same term (Fig. 2A). The “between process” category received a count for any combinations that were not counted for within process (Fig. 6B). For all digenic interactions, annotations for the query gene and the

identified interacting genes were considered; *HO* is a benign control locus that houses the marker and it is excluded from the analysis. For each biological process, trigenic vs. digenic fold change was also calculated and represents the ratio of trigenic interaction enrichment relative to digenic interaction enrichment.

Digenic and trigenic interactions were tested for overlap with several functional standards: protein-protein interactions, GO biological process, co-expression and co-localization. A hypergeometric test of the overlap between interactions and functional annotations, in the space of gene pairs that are both in the standard and have a valid (non-NaN) SGA score, was used to evaluate statistical significance (Fig. 2B, S8B). Digenic interactions whereby both genes were annotated to the same term within a particular functional standard or trigenic interactions whereby all three genes were annotated to the same term within a particular functional standard were used to test the overlap. Digenic interactions ($\varepsilon < -0.08$, $p < 0.05$) and trigenic interactions ($\tau < -0.08$, $p < 0.05$) were used for this analysis.

Trigenic interactions were considered to overlap with a protein-protein interaction, if both genes deleted from the query strain encode for proteins that interact with the protein encoded by the array gene in the protein-protein interaction standard merged from several sources (56-60), similarly digenic interactions were considered to overlap with a protein-protein interaction if both the protein encoded by a query gene showed a protein interaction with a protein encoded by an array gene.

For digenic and trigenic interactions, both genes or all three genes, respectively, were considered true positives for co-annotation, if they are co-annotated to a GO term that is enriched on the global genetic interaction profile similarity network (7,55) and true negatives if they are not co-annotated to a common GO term.

For digenic and trigenic interactions, both genes or all three genes, respectively, were considered true positives for co-expression, if their MEFIT co-expression scores exceeded 1.61 (97th %) and were considered true negatives if their MEFIT co-expression scores fell below -0.17 (50th %) (61).

For digenic and trigenic interactions, both genes or all three genes, respectively, were considered true positives for co-localization, if they shared at least one cellular localization pattern and true negatives if they shared no cellular localization pattern given binary localization assignments that were based on previously reported LOC-score cutoffs (62). For all digenic interactions, annotations for the query gene and the identified interacting genes were considered; *HO* is a benign control locus that houses the marker and it is excluded from the analysis.

Subclassification of negative trigenic interactions, as described in the section above ‘Classifying trigenic interactions into novel vs. modified,’ enabled us to test if they significantly overlapped the aforementioned functional standards (Fig. S8B). We observed that ‘novel’ negative trigenic interactions show no significant enrichments with the exception of the co-annotation standard. This indicates that ‘novel’ trigenic interactions connect functionally distant genes and/or carry less functional information. In contrast, ‘modified’ trigenic interactions are similar to digenic interactions and connect more functionally related genes, significantly overlapping with most of the tested functional standards. ‘Modified’ trigenic interactions with at least 1 negative digenic interaction and no positive digenic interactions are enriched for an overlap with all functional standards except for protein-protein interaction standard, indicating that in

these cases a third perturbation exacerbates a double mutant effect of a gene pair with which it exhibits a functional relation but does not involve protein complex members or other interacting proteins. However, ‘modified’ trigenic interactions with only positive digenic interactions show a marked increase in the overlap with the protein-interaction standard as well as other standards, suggesting that in these cases a third perturbation connects genes whose protein products interact or belong to protein complexes. Thus, trigenic interactions can serve as important phenotypic modifiers in different genetic backgrounds.

Morphology of secretory pathway compartments and peroxisome biogenesis

Strains deleted for *MDY2*, *MTC1* or *MDY2+MTC1* and expressing Pex14-GFP, Sec63-GFP, Cop1-GFP or Sec7-GFP were grown to mid-log phase at room temperature in synthetic dextrose media lacking tryptophan (SD-Trp) to minimize background fluorescence (Fig. 5B, S9B). Subcellular compartment morphology was assessed using a spinning-disc confocal microscope (WaveFX, Quorum Technologies) connected to a DMI 6000B fluorescence microscope (Leica Microsystems) controlled by Volocity software (PerkinElmer), and equipped with an Imagem charge-coupled device camera (Hamamatsu C9100-13, Hamamatsu Photonics) and 63x/NA1.4 Oil HCX PL APO objective. Imaging was done at room temperature. 21 optical sections encompassing the whole cell were imaged at intervals of 0.3 μm . Images were processed using ImageJ. Data shown are the average of three independent experiments.

Endocytic membrane trafficking assays using Sla1-GFP dynamics

Strains deleted for *MDY2*, *MTC1* or *MDY2+MTC1* and expressing Sla1-GFP were grown to mid-log phase, immobilized on concanavalin A-coated coverslips, and sealed to standard glass slides with vacuum grease (Dow Corning). Images were acquired on the microscope setup described above at room temperature for 3 minutes at a rate of 1 frame/second and processed and analyzed using ImageJ (<http://imagej.nih.gov/ij/>). 100 patches from 10-20 cells were analyzed per strain in two independent replicates (Fig. 5A).

DNA damage sensitivity assays

Yeast strains (WT: Y13096, *mdy2* Δ : TM2745, *mtc1* Δ : TM3060, *mdy2* Δ *mtc1* Δ : TM2430) were grown overnight in YPD, serially diluted, and spotted onto YPD plates containing the indicated concentrations of HU (Bio Basic Canada) or MMS (Sigma-Aldrich) (Fig. 5C, S10A&F). Plates were incubated at the indicated temperatures for 2-4 days. The *rtt107* Δ mutant has a known fitness defect on media containing HU or MMS (70). BY4741 was added as a control for the background of *rtt107* Δ . Refer to Additional Data S3 for complete strain genotype details.

Flow cytometry, whole cell extracts, and immunoblotting

Logarithmically growing cells at 30°C were treated with 200 mM HU for 1h, harvested, washed with YPD, and released into fresh YPD to recover for 60 minutes. Cultures were sampled at the indicated times and either (i) processed for flow cytometry as previously described (71) or (ii) fixed with 10% trichloroacetic acid before preparation of whole cell extracts (72). DNA contents were measured using a FACS Calibur flow

cytometer, and data were plotted as histograms using FlowJo Flow Cytometry Analysis Software, version 10.0.8 (Fig. S10B). Proteins from whole cells extracts were resolved by SDS-PAGE and subjected to immunoblotting with α Rad53 (abcam ab104232), α H2A-S129-P (abcam ab15083), or α PGK (Novex #459250) antibodies (Fig. S10C).

Functional annotation of digenic and trigenic interactions using SAFE

SAFE (Functional annotations based on the Spatial Analysis of Functional Enrichment) of the global genetic interaction profile similarity network were used to annotate gene function in this study (7,55). For the gene pair in each query strain, their digenic interactions and trigenic interactions identified at the intermediate threshold (ϵ or $\tau < -0.08$, $p < 0.05$) were taken as inputs to SAFE analysis. An enrichment score was calculated for each gene on the global similarity network from theCellMap.org (27) based on the overlap of its direct neighborhood with the given digenic/trigenic interactions. The enrichment significance was evaluated by the hypergeometric test. The set of digenic interactions of each gene in the query pair was assessed independently (Fig. 4B-D, Fig. S10E). The corresponding enriched bioprocess clusters were visualized on theCellMap.org and the most diverged digenic interaction profiles compared to trigenic profiles are depicted in Fig. 4B-D, S11D.

Bicluster analysis

To identify genes that might mediate the connection between the *MDY2* and *MTC1* genes that are primarily associated with vesicle trafficking roles and the DNA replication defect that is observed in the double mutant, we used bicluster analysis to search for single query genes with digenic interaction profiles resembling the DNA signature embedded within the double mutant *mdy2 Δ mtc1 Δ* trigenic interaction profile. Trigenic genetic interactions were restricted to those residing in the DNA replication/repair SAFE cluster on the global similarity network (7) and bicluster analysis was performed as previously described in (71) (Fig. S10D). They involved genes with roles in DNA replication and repair and TOR2 signaling suggesting that the *mdy2 Δ mtc1 Δ* double mutant is partially defective for TOR2 function, consistent with emerging evidence of a link between TOR2 and DNA replication and repair (73); however, the defect in Tor2 function is partial and relatively weak since the *MDY2-MTC1* double mutant query shows a relatively weak synthetic sick trigenic interaction with *TOR1*.

Metabolomic analysis

To further investigate the functional connection of *MDY2* and *MTC1* to DNA replication and repair we used untargeted full scan metabolomics to capture the metabolic functions of *mdy2 Δ* , *mtc1 Δ* and *mdy2 Δ mtc1 Δ* deletion mutants. Prototrophic yeast deletion mutants, *mdy2 Δ* , *mtc1 Δ* , *mdy2 Δ mtc1 Δ* , were constructed by transformation and selection of deletion alleles from the yeast deletion collection into the prototrophic haploid background (74). The *mdy2 Δ* (Y14965), *mtc1 Δ* (Y14968), *mdy2 Δ mtc1 Δ* (Y14978) deletion strains and wild-type control (FY4) were grown in minimal media (1.7 g/L yeast nitrogen base without amino acids or ammonium sulfate (BD Difco), 1.0 g/L monosodium glutamate, 20 g/L D-glucose). Refer to Additional Data S3 for complete strain genotype details. For each strain, six independent cultures were inoculated in 24-well plates containing 5 mL minimal media and grown overnight at 25 °C. The following

day, cells were sub-cultured with sufficient cell density to reach a target OD of ~1 by morning. The next morning, cells were sub-cultured to reach a target OD of ~0.5 at time of extraction. Sub-cultured cells were grown for 4 hours at 25 °C, followed by 2 hours at 37 °C. The *mtc2Δ*, *mtc4Δ*, *mtc6Δ* and *may24Δ* metabolite extracts were prepared as previously described (7). Full-scan mass spectra acquired in profile mode were analyzed by extracting peak intensities followed by manual integration of peak areas. As each sample was spiked with stable isotope labeled yeast metabolite extract, each metabolite peak area is normalized to a co-eluting peak present in the ¹³C ¹⁵N reference yeast internal standard. Metabolite levels are expressed as a ratio of unlabeled to stable-isotope labeled, normalized to wild-type control, and expressed on the log₂ scale. Each data point represents the mean of 4-6 independent biological replicate cultures. The *mdy2Δ mtc1Δ* double mutant has elevated levels of metabolites involved in de novo biosynthesis of NAD⁺ from kynurenine (Fig. S10G&H), which is involved in telomere uncapping (7, 75, 76) and possibly influences DNA synthesis pathways.

Functional diversity of digenic vs. trigenic interaction profiles

Genetic interaction profile similarity for gene pairs were used to indicate functional diversity and were taken from (7). All pairs of genes that exist in the trigenic interaction data experiment (as a query or array) were placed into four mutually exclusive categories: i) a pair of genes that exhibits a digenic interaction, ii) a pair of genes that participates in a modified trigenic interaction, but do not themselves interact, iii) a pair of genes that participates in a novel trigenic interactions, and thus by definition do not interact digenically, iv) a pair of genes that share no interaction of any type (random background). Pairs of genes which fall into more than one of these categories are placed into the first matching category according to the precedence described here. Statistical significance between distributions of genetic interaction profile similarity scores was calculated using a Wilcoxon rank sum test as implemented in MATLAB (Fig. 6A, S11A).

We also did a systematic evaluation of the functional diversity of digenic vs. trigenic interactions using connected component analysis. To ensure an unbiased comparison, we excluded queries that displayed less than 10 digenic or trigenic interactions in our analysis. For the remaining 59 double mutants and their corresponding single mutant control strains, the functional diversity of trigenic or digenic interactions was measured by the number of enriched bioprocesses (enrichment score $p \leq 0.05$). First, we restricted our analysis to enriched genes that resided within large gene clusters, which are characterized by greater than 20 genes and in which genes are mostly annotated to a neighborhood of a specific bioprocess, by using connected component analysis (55). Second, we identified bioprocesses with significantly enriched digenic/trigenic interactions, if there was a significant number of interacting genes in the cluster that was annotated to a specific bioprocess rather than spanning multiple bioprocesses, with the minimum number of enriched genes equal to 10 and percent of such genes in the cluster equal to 15%. A signed-rank test was used to determine whether trigenic interactions were annotated to a higher number of bioprocesses than their corresponding digenic interactions (Fig. 6C). We showed that the results of this test are robust by exploring combinations of several parameters for the bioprocess assignment: minimum number of enriched genes: 5 - 20, and percent of such genes in the cluster: 10 - 50% (Fig. S11B) and the subtraction approach for scoring trigenic interactions (Fig. S11C).

Extrapolation of the global trigenic interaction network

To estimate the number and density of trigenic interactions across the entire yeast genome space, we employed the following procedure (see also the main text). Briefly, we first binned our experimental double mutant queries into three bins along each of three axes that show individual relevance to the prediction of trigenic interaction degree (Fig. 7A, Table S1, Additional Data S7). Next, we estimated the average trigenic interaction degree for double mutant queries in each bin. Then, we assigned all possible gene pairs to the appropriate bin given known pairwise characteristics from the digenic interaction network (7). Finally, we multiplied the expected number of trigenic interactions for each bin (the experimental mean) by the number of genome pairs assigned to that bin to obtain a final estimate (Fig. 7D, S14, S15, Table S3). In summary, for the extrapolation, we predicted the trigenic degree only for the portion of double mutants with a specified set of characteristics, therefore preserving the distribution of all the double mutants across the digenic interaction features.

Binning double mutant query pairs

All double mutant queries were binned into a total of 27 bins according to three parameters (Fig. 7A, Table S1, Additional Data S7), all of which correlate with trigenic interaction degree (Fig. S12): i) digenic interaction score between constitutive single mutants (bin thresholds: 0, -0.08, -0.1, $-\infty$); ii) average digenic interaction degree of constitutive mutants (bin thresholds: 10, 45, 70, $+\infty$); and iii) digenic interaction profile similarity (bin thresholds: -0.02, 0.03, 0.1, $+\infty$). All three of these measures are derived from an independent survey of digenic interaction space (7). Specifically, i) digenic interaction score between constitutive single mutants was taken from (7), matching exact strains were available (Additional Data S7), otherwise using ORF based match, if multiple interactions are available for a given pair, their mean is used; ii) average digenic interaction degree of individual genes of the pair was calculated by taking the mean of digenic degree at the negative intermediate cut-off ($\varepsilon < -0.08$, $p < 0.05$) using appropriate query strains that were screened against the genome-wide array of non-essential gene deletion mutants (7) (Additional Data S7) and iii) digenic interaction profile similarity was taken directly from (7) and represents a standard integrated over multiple experimental contexts (Additional Data S7). The same procedure governs the binning of the experimental double mutant queries and the binning of all gene pairs as potential double mutant queries for the estimation of the total number of negative trigenic interactions in the yeast genome. Gene pairs with values that fall outside the bin ranges, or those that have missing values, are placed in a fourth bin along the given axis. For these purposes, missing/out-of-range value bins were considered to have the following thresholds: digenic profile similarity: $(-\infty, -0.02)$, digenic interaction strength: $(0, +\infty)$. We therefore provide one set of conservative estimates for those gene pairs which fall in the regions mapped by our 3x3x3 bins (Fig. 7D, Fig. S14, Fig. S15A Table S3 (conservative)), and another set that includes trigenic interactions from (and extrapolates trigenic interactions to) all pairs in the genome, including those that fall outside the main 27 bins (Fig. S15B, Table S3 (genome-wide)).

Query genes were also sampled from different biological processes. Broadly defined bioprocess categories were derived from (15) and query genes were sequentially

taken from different bioprocess categories to populate each bin. To make general predictions about the trigenic interaction space, the query gene set was restricted to unambiguous singletons that did not identify as duplicated genes as defined in (77).

Establishing the expected trigenic interaction degree for each bin

Within each bin we estimate the expected trigenic interaction degree by taking the mean trigenic interaction degree of the experimental double mutant queries assigned to that bin. Fig. 7A shows in dark blue the bin with the highest average trigenic interaction degree of 63.5. In missing value cases, where no experimental pairs have been assigned to a bin (e.g. due to bootstrap sampling, see below) we fill in the missing value using the mean values from all available adjacent bins (up to two in each dimension for a maximum of six possible). As the experimentally observed trigenic interaction degree was gathered from an array of only 1,182 genes, we calculated the interaction density of each hypothetical query, and then multiplied that density by the size of a hypothetical full-genome array; expanding the degree in each query by a factor of 5794/1182.

Extrapolation of degrees for all pairs

Finally, we counted the total number of gene pairs in the genome that would fall into each bin based on their properties using the global digenic interaction network (7), and multiplied it by the expected trigenic interaction degree for that bin. Here, we used the space of 5,794 genes for which there is sufficient digenic data to represent the genome. As each trigenic interaction involves three genes, and we are summing over the degrees of all possible double mutant queries, we divide the final result by three to compensate for the number of possible two-gene queries that could capture each interaction. The entire process is repeated using two established thresholds for scoring genetic interactions (ϵ or $\tau < -0.08$, $p < 0.05$ and ϵ or $\tau < -0.2$, $p < 0.05$). To establish confidence intervals, the extrapolation process was repeated with 10,000 boot-strapped samplings of the 151 double mutant query pairs, their associated trigenic interactions degrees, and corresponding digenic interaction features (Fig. 7D, Fig. S14, Fig. S15, Table S3).

Estimation of the global digenic interaction network

Previous work has mapped the properties of digenic interaction space extensively, including estimates of precision and recall of a representative set of query screens (7). We used this information to bound the potential number of real digenic interactions, according to the following procedure. Per-screen estimates of precision and recall were obtained for 14 query mutants crossed into an array of temperature sensitive mutants of essential genes, and also for 26 query mutants crossed into an array of nonessential gene deletion mutants (7). Our analysis indicates that the precision of a given query (where true positives are defined as interactions that show up in two or more replicates) is well approximated by a function of its interaction degree: $precision = \frac{\log(degree)}{7}$. Whereas the recall characteristic shows no association with degree, and is instead approximately normal with a mean of 0.56 and a standard deviation of 0.2. To generate an estimate of the total number of digenic interactions in the dataset, we take a bootstrapped sample of the observed degree distribution, and calculate the query-wise number of true positive interactions by applying the formula for precision and multiplying by the bootstrapped

degree. Each query is assigned a random recall value drawn from the normal distribution (0.56, 0.2) and the total number of real interactions (true positive + false negative) for each query is calculated as the number of true positives divided by recall. This measure is summed over all queries in the bootstrapped sample to estimate the total true interactions in the dataset, and the entire procedure is repeated 50,000 times to generate the distributions shown in Fig. 7D and Fig. S15.

Parametrizing Dobzhansky-Muller Incompatibility Models

A common explanation for the genetic basis of speciation is the Dobzhansky-Muller Incompatibility (DMI) model. This model postulates that hybrids between two diverged populations may experience reduced fitness due to novel negative genetic interactions (epistatic) that occur between loci with fixed differences between the parental populations (78-80). Mathematical theory predicts that these negative effects add up exponentially as species diverge, resulting in the “snowball” hypothesis for hybrid incompatibilities (36). Using empirically measured strengths and abundances of both digenic and trigenic interactions, we can make some tantalizing predictions about the relative importance of simple vs. complex interactions in causing speciation. While knockout mutations are unlikely to represent the fitness effects caused by the average mutation in a natural population, and our experimental design is inherently underpowered in detecting interactions of weak effect, we can nonetheless say something about interactions of large effect.

Modifying the Turelli and Orr DMI model (81) slightly to account simultaneously for both digenic and trigenic interactions, we can show that the fitness of a hybrid (W_H) after a total of K substitutions have been fixed is:

$$W_H(K) = e^{p_2 \binom{K}{2} + p_3 \binom{K}{3}}$$

Where p_2 is the average fitness decrease in hybrids compared to the parental populations due to any randomly chosen digenic interaction, p_3 is the average fitness decrease in hybrids due to trigenic interactions, and $\binom{K}{n}$ is the binomial coefficient K choose n representing the number of ways to choose a set of n loci from the K fixed substitutions. The two parameters of interest, p_2 and p_3 can be broken down into two components – the probability that an interaction exists (α_2, α_3) times the average effect of an interaction (ϵ_2, ϵ_3), as in (82). Using the empirical measurements from our network, we can obtain several different values for each. Table S4 lists the different estimates of α_2 , and α_3 . Among those interactions, digenic interactions are generally stronger, with the average measured negative trigenic interaction being about 25% weaker than digenic interactions. Since these interactions are quite strong, speciation by knockouts would be expected in general within 20 fixed differences between populations as depicted in Fig. S16A.

An additional question we may ask is what proportion of reproductive incompatibilities in the hybrid is caused by digenic vs. trigenic interactions. To model this, we define the proportion of fitness defect (load) due to trigenic interactions. We assume that a hybrid population experiencing no deleterious genetic interactions (epistasis) would have a relative fitness of 1. The hybrid load is, then, defined simply as $1 - W_H(K)$. Hybrid load due to trigenic interactions alone is given by $1 - e^{p_3 \binom{K}{3}}$. The proportion of load due to trigenic interactions is therefore:

$$L_3 = \frac{1 - e^{p_3 \binom{K}{3}}}{1 - e^{p_2 \binom{K}{2} + p_3 \binom{K}{3}}}$$

While the relative importance of trigenic interactions varies based on our assumptions about their relative abundances, in general hybrid fitness becomes largely determined by trigenic rather than digenic interactions as shown in Fig. S16B. As noted, this may be an artifact of the relatively large size of interactions in general.

If, for example, we were to use the mean of all significant, negative ε_2 , ε_3 values, we also find that trigenic interactions are weaker in comparison to their digenic counterparts. We find that for the total trigenic network, the ratio of p_3 to p_2 is approximately 0.12. Extrapolating to the nearly complete digenic network measured in Costanzo *et al.* (7), we may ask whether fitness would decrease as rapidly when the average effect is not as extreme. We accordingly use three estimates of p_2 from the Costanzo *et al.* (7) network taking into account false positive and false negative rates ($p_2 = -0.0015$ (low end), -0.003 (median), -0.006 (high end)) and scale p_3 by the ratio measured from the trigenic network. Under such assumptions, hybrid fitness decreases far more slowly (Fig. S16C) but hybrid fitness remains largely determined by trigenic rather than digenic interactions (Fig. S16D). It is important to note that it may not be possible to extrapolate the total trigenic network from the data presented here; however, the relative strengths and probabilities of digenic and trigenic interactions do suggest that complex incompatibilities may be an important contributor to speciation.

Estimation of the minimal yeast genome by accounting for digenic interactions

We estimated the size of the yeast minimal genome after accounting for the global set of digenic interactions described in our recent study (7). The basic rationale of our estimation procedure was to select a minimal set of genes such that no pair of genes with a genetic interaction resulting in a significant fitness defect was simultaneously excluded from the minimal genome. The minimum allowable fitness defect was a parameter in the analysis and was varied between 0.1 and 0.9. We used the complete set of digenic interactions from (7) defined at the intermediate confidence threshold ($\varepsilon < -0.08$ and $p < 0.05$).

For a given choice of the minimum allowable fitness parameter, we ran the following algorithm to estimate the minimal genome. First, all essential genes were added to the minimal genome set. We then used a greedy algorithm to select nonessential genes to satisfy the constraints defined by digenic interactions. Specifically, for each iteration, we added the single nonessential gene that occurred in the largest number of unsatisfied digenic genetic interactions for which the double mutant fitness was below the minimum allowable fitness threshold. This process was repeated until all digenic interactions were satisfied, at which point the selected set was considered the minimal genome. This process was then repeated for a range of settings of the minimum allowable fitness defect (between 0.1 and 1 in increments of 0.1). The resulting minimal genome sizes are presented in Table S5.

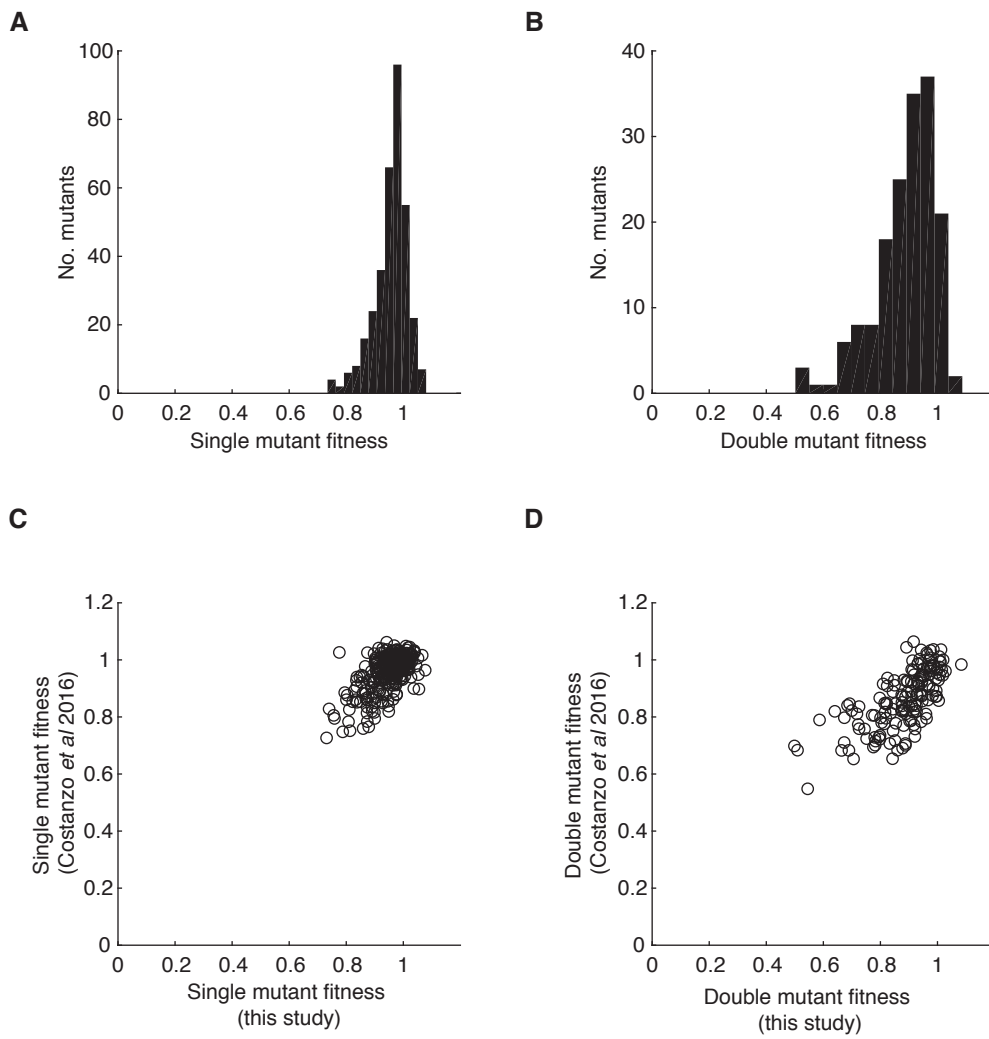


Fig. S1. Quantification of fitness of query strains using high-density arrays and comparison to published data. (A) Histogram of single mutant fitness estimates of all single mutant control query strains used in this study, $n = 342$. (B) Histogram of double mutant fitness of all double mutant query strains used in this study, $n = 165$. (C) Scatter plot comparing the single mutant fitness derived from this study and another study (7), $n = 331$, $r = 0.63$, $p = 0$. (D) Scatter plot comparing double mutant fitness derived from this study and another study (7), $n = 153$, $r = 0.69$, $p = 0$. r denotes Pearson correlation coefficient.

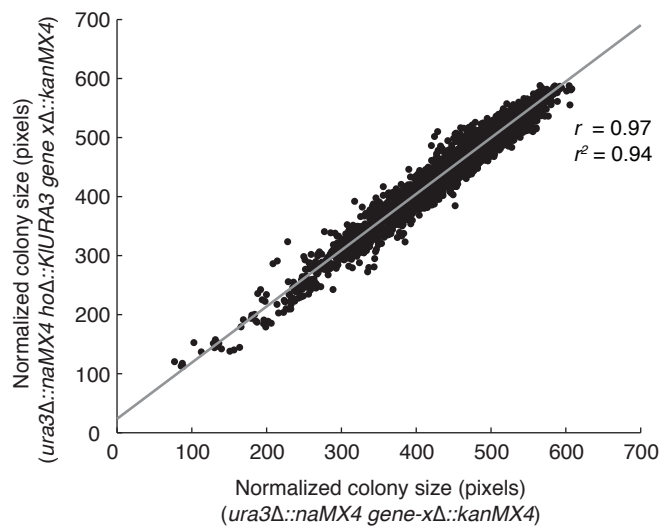


Fig. S2. Negligible effect on fitness of *hoΔ*. Correlation of normalized colony sizes (in pixels) derived from the single mutant screens using the query strain *ura3Δ::natMX4* ($n = 71$) from a previous study (7) and the single mutant screens using the query strain *ura3Δ::natMX4 hoΔ::KIURA3* ($n = 7$) crossed to the genome-wide array of non-essential gene deletion mutants ($xΔ::kanMX4$). The average Pearson correlation coefficient is 0.97.

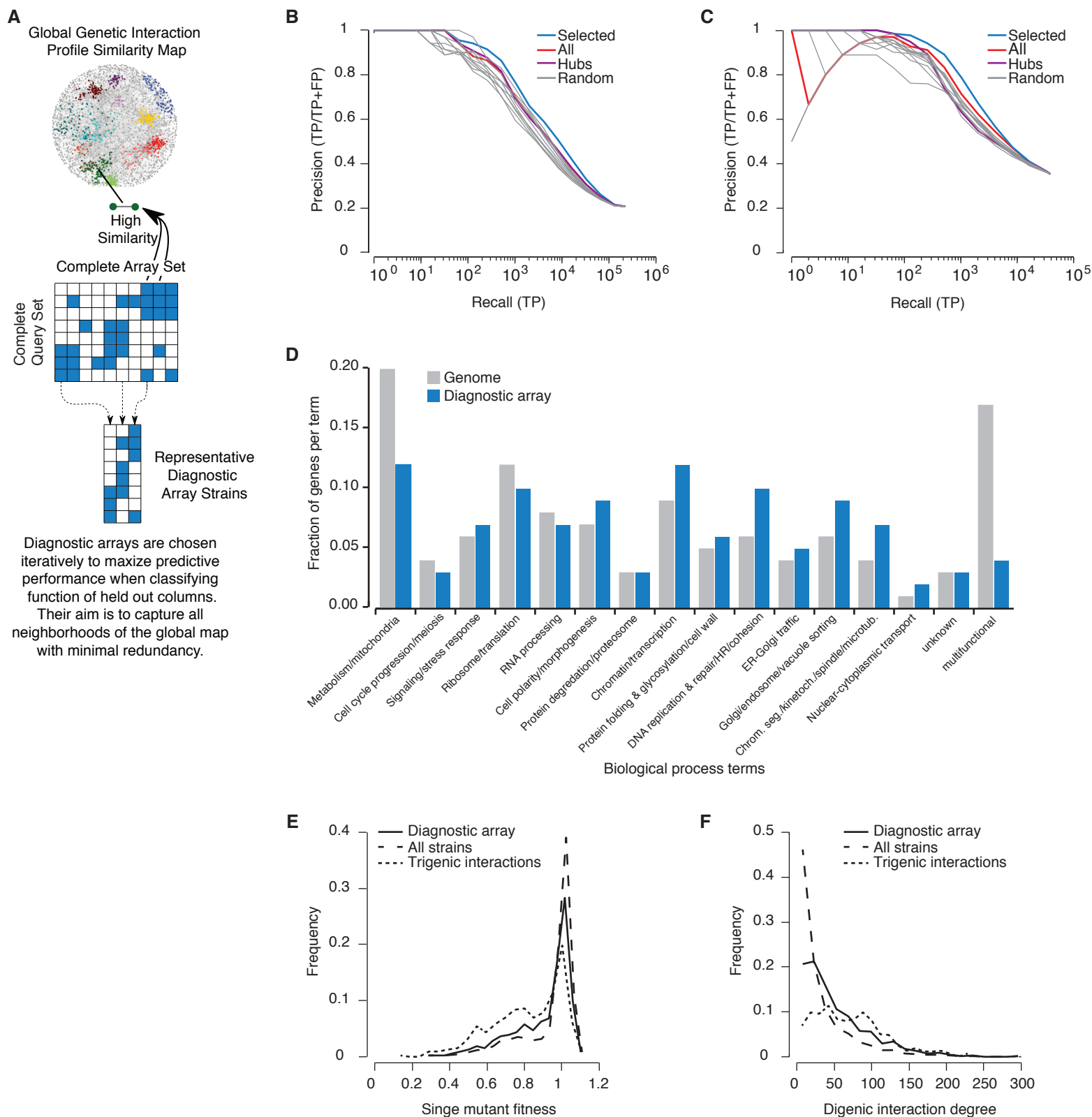


Fig. S3. Diagnostic array characteristics. (A) An illustration of the COMPRESS-GI method for selecting diagnostic array strains. Diagnostic array strains are chosen iteratively to maximize predictive performance when classifying function of held out columns. The aim is to capture all bioprocesses on the global genetic interaction similarity map with minimal redundancy. (B-C) The ability of 990 non-essential gene deletion mutants (B) and 192 temperature sensitive alleles of essential genes (C) to re-cluster the digenic interaction profile correlation matrix. A true positive (TP) was defined as a gene pair, which has high genetic interaction profile similarity and is co-annotated to the same GO biological process term. Selected diagnostic array genes maximized the precision-recall curve compared to randomly selected sets, genetic interaction hubs or all gene mutants present on the genome-wide array. Precision and recall were calculated as previously described (68). Refer to (16) for diagnostic array details. (D) Fraction of genes annotated to previously described biological processes (15) for genes represented by mutant strains on the diagnostic array and across the entire genome. (E-F) The diagnostic array captures the distribution of (E) single mutant fitness estimates and (F) digenic interaction degree of array strains that exhibit trigenic interactions in pilot experiments. 'Diagnostic array' includes strains that are found on the diagnostic array; 'All strains' includes all essential and non-essential gene mutants on genome-wide deletion and TS mutant arrays (7); 'Trigenic interactions' include mutant strains that showed trigenic interactions in pilot experiments, $\varepsilon < -0.08$, $p < 0.05$.

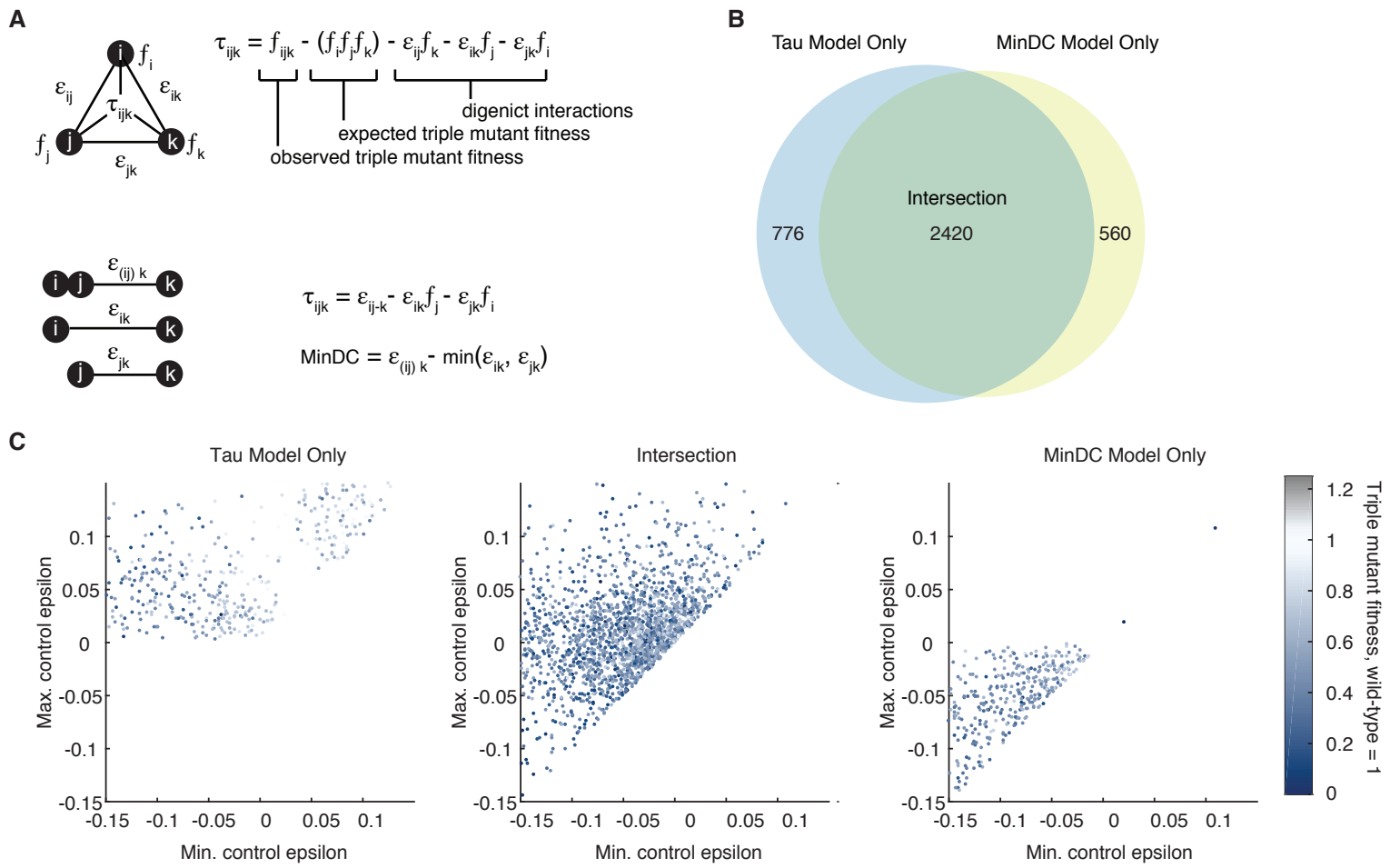


Fig. S4. Comparison of τ -SGA to MinDC score approaches for quantifying trigenic interactions. **(A)** Trigenic interaction models. Symmetric theoretical model is shown above and corresponding asymmetric models for τ -SGA and MinDC are shown below. **(B)** Data for 182 double mutant queries (and 364 associated single mutant controls) were reassessed using the MinDC model. Venn diagram shows the number of significant negative trigenic interactions under each model. The majority of interactions receive a significant score under either model. **(C)** Each plot shows a set of significant trigenic interactions ($\tau \leq -0.08$, $p < 0.05$) corresponding to one section of the Venn diagram in B. Each point represents an interaction with the smaller (more negative) digenic control epsilon on the X-axis, and the other (max) control epsilon on the Y-axis. The color of the point corresponds to the fitness of the triple mutant (relative to wild-type) which is not affected by the choice of model. MinDC subtracts only the more extreme of the scores from the two single mutant control queries for a given interaction. Thus, under the MinDC model, triple mutants that combine multiple negative epistatic effects to result in a severe phenotype, may be called trigenic despite the fact that the phenotype can be explained by the comprising digenic interactions. Refer to (16) for model comparison details.

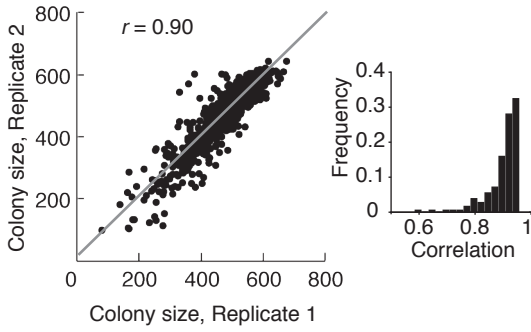
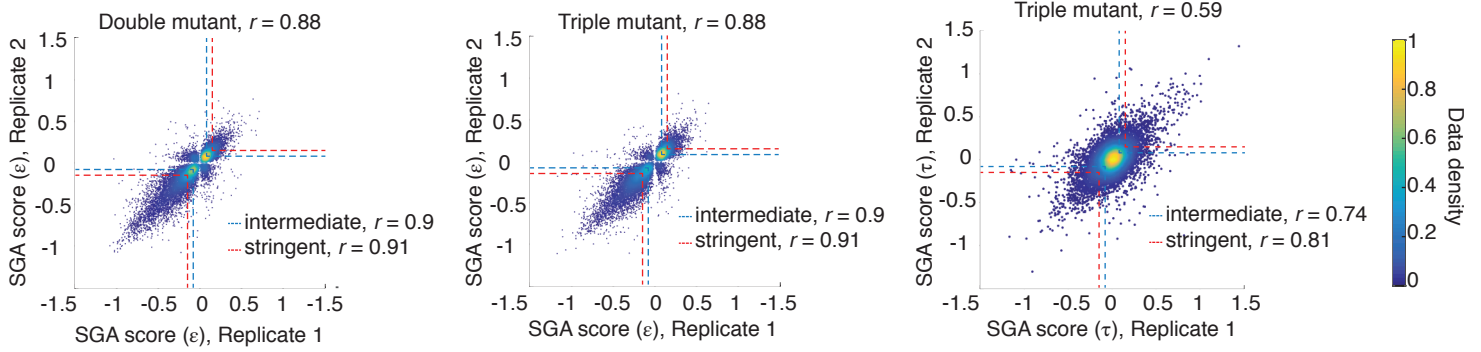
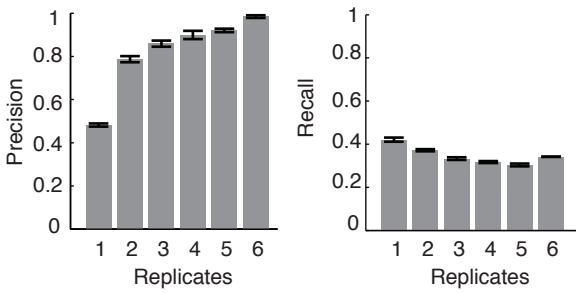
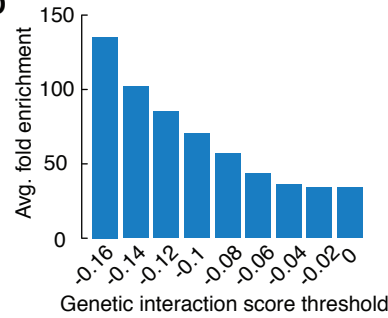
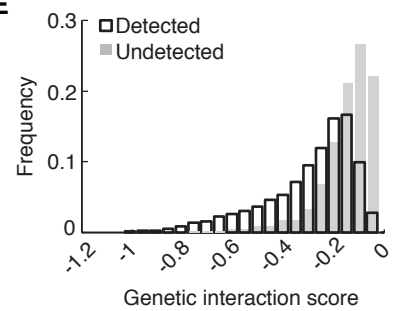
A**B****C****D****E**

Fig. S5. Reproducibility of genetic interactions depends on their magnitude. (A) Correlation of triple mutant fitness measures obtained from two independent replicates of a representative screen. The line of best fit is shown in red. Inset: The distribution of correlations between triple mutant fitness measures ($n = 172$). **(B)** Correlation of double (left), raw triple (middle) and adjusted triple (right) mutant interaction scores from two independent replicates. Significant interactions scores ($p < 0.05$) are shown; the dashed lines represent intermediate, $I_{\text{score}} > 0.08$, $p < 0.05$ (blue) and stringent, $I_{\text{score}} > 0.12$, $p < 0.05$ (red), cut-offs. **(C)** Replicate analysis. Precision and recall are calculated based on a 'Gold Standard' of true positives that consists of any interaction called significant at the intermediate threshold, $\epsilon < -0.08$, detected in at least two replicates. Queries ($n = 31$) are scored with varying number of replicates using the established SGA score method (8). **(D)** Control digenic interaction screens ($n = 20$) with 4 replicates were combined in random pairing of 2 replicates and scored. Average fold enrichment for overlapping significant negative genetic interactions averaged across 3 combinations of data sets are shown. X-axis shows the threshold that was used to evaluate the significant negative genetic interactions, $p < 0.05$. Interactions with a stronger magnitude are more likely to be detected in both replicates. **(E)** Distribution of digenic interactions that are either detected or undetected in unadjusted triple mutant screens. Digenic interactions that are undetected in raw triple mutant screens tend to be weaker in magnitude, consistent with the higher reproducibility of stronger interactions in replicate screens shown in (D). Refer to (16) for reproducibility analysis details.

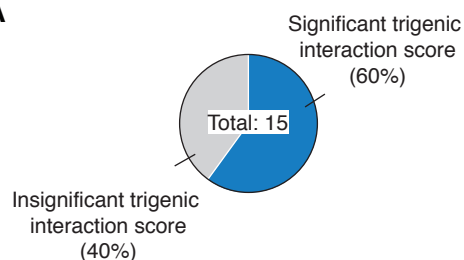
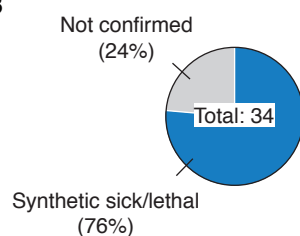
A**B**

Fig. S6. Confirmations by tetrad and random spore analyses. (A) Pie chart showing the number of high-confidence trigenic interactions reported in a previous study for *cln1Δ cln2Δ* double mutant query (19) that were scored as significant or insignificant trigenic interactions in this study. **(B)** Pie chart showing the number of trigenic interactions for *cln1Δ cln2Δ* double mutant query that were not previously reported in (19) but were confirmed by random spore analysis. See Table S2 for confirmation results and (16) for validation details.

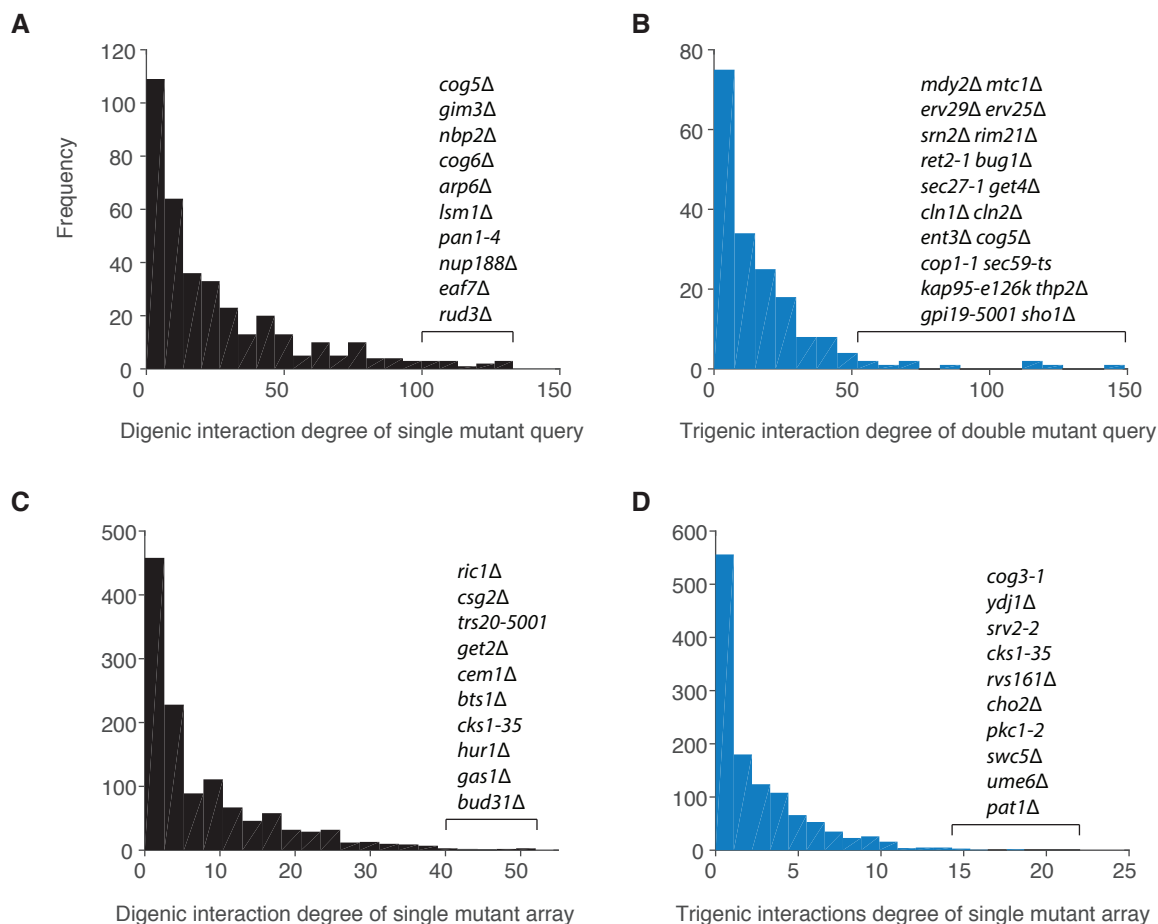


Fig. S7. Distribution of digenic and trigenic interactions for query and array mutants. **(A)** Histogram showing the distribution of digenic interaction degree of single mutant queries. **(B)** Histogram showing the distribution of trigenic interaction degree of double mutant queries. **(C)** Histogram showing the distribution of digenic interaction degree of single mutant arrays. **(D)** Histogram showing the distribution of trigenic interaction degree of single mutant queries. Ten mutants with the highest degrees are listed in their corresponding panels.

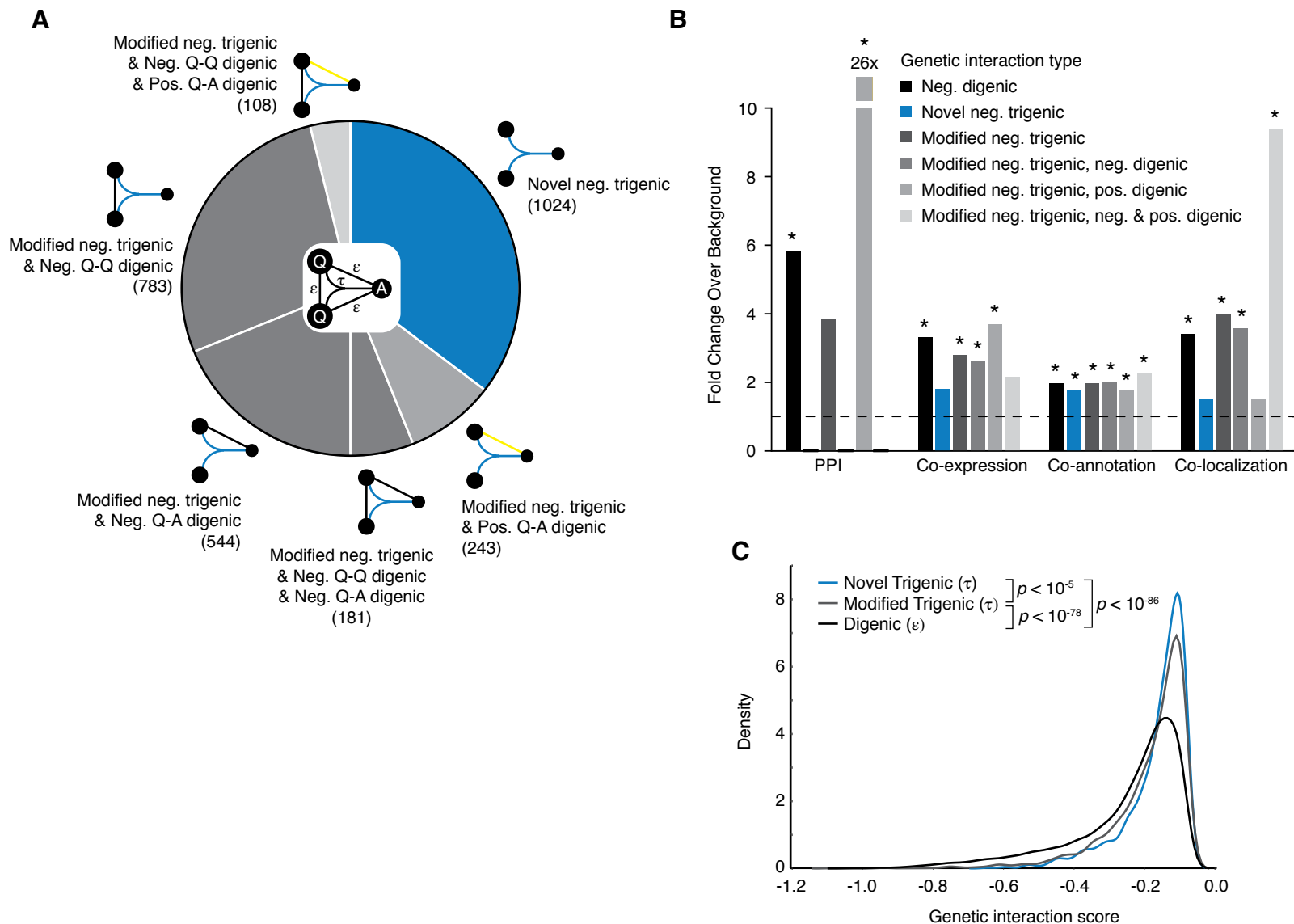


Fig. S8. Features of modified and novel trigenic interactions. (A) Pie chart depicting the total number of trigenic interactions of different classes. A trigenic interaction between a double mutant query and the array strain is called *novel* (blue) if there is no significant digenic interaction between either single mutant control query and the array strain or between the query gene pair. Trigenic interactions that overlap with one or more negative or positive digenic interactions are called *modified* (grey), and are further classified by the type of the digenic interaction. Of our 182 double mutant query strains, 34 show a negative digenic interaction between query gene pair (black Q-Q), thus all trigenic interactions of these queries are *modified*. Interactions may further be classed by digenic interactions (if any) between a single mutant query control strain and the array strain (black Q-A negative, yellow Q-A positive). **(B)** Enrichment of negative trigenic interactions across four functional standards. The functional standards are the following: merged protein-protein interaction (PPI) standard, co-annotation to GO biological process, co-expression, co-localization. The dashed line denotes background expectation. Several similar classes from panel (A) have been collapsed. Colors as in panel (A), with functional enrichments for all digenic interactions of single mutant control query strains shown for comparison. Bars marked with an asterisk (*) designate categories with significant overlap with a functional standard (hypergeometric $p < 0.05$). **(C)** Distribution of magnitudes for digenic (black), novel trigenic (blue) and modified trigenic (grey) interactions. Pairwise significance was assessed using a Wilcoxon rank-sum test. Refer to (16) for classification and functional analysis details.

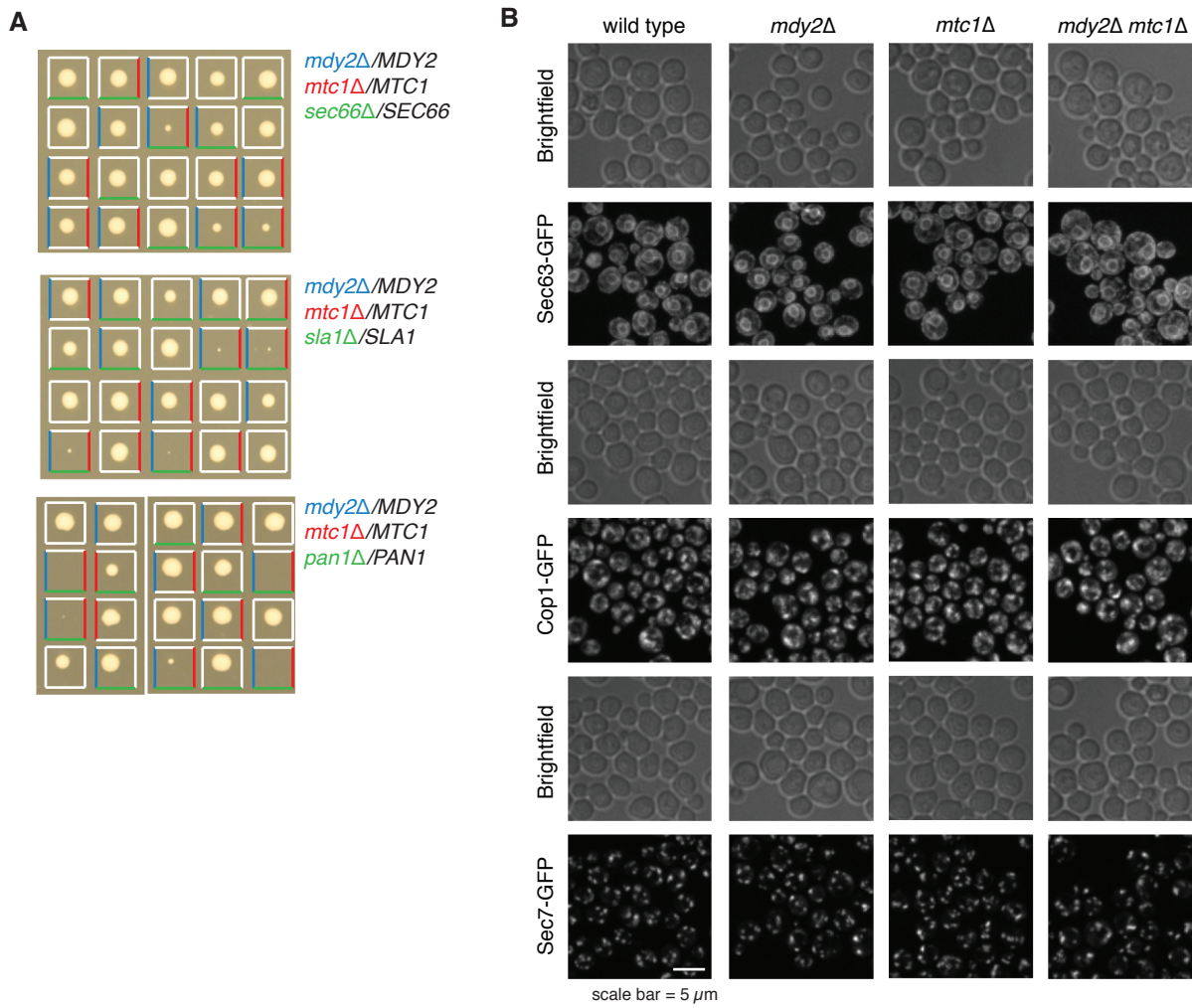


Fig. S9. Endocytic membrane trafficking and peroxisome biogenesis are impaired in *mdy2Δ mtc1Δ* double mutant. (A) Examples of *mdy2Δ mtc1Δ* trigenic interactions that were validated by tetrad analysis. Blue - *ura⁺* (*mdy2Δ*), Red - *natR* (*mtc1Δ*), and green - *kanR* (*sec66Δ*, *sla1Δ*, *pan1Δ*). Spores from a single tetrad are oriented vertically. For the complete list of trigenic interactions that were validated for *mdy2Δ mtc1Δ* by tetrad analysis see Additional Data S6. **(B)** Representative fluorescent micrographs of wild-type, *mdy2Δ*, *mtc1Δ* and *mdy2Δ mtc1Δ* mutants yeast cells expressing a GFP-tagged protein localized to the ER or the Golgi. All strains exhibit wild-type morphology of cellular compartments along the steps of the early secretory pathway. Sec63-GFP was used to mark the ER, Cop1-GFP and Sec7-GFP to mark the Golgi.

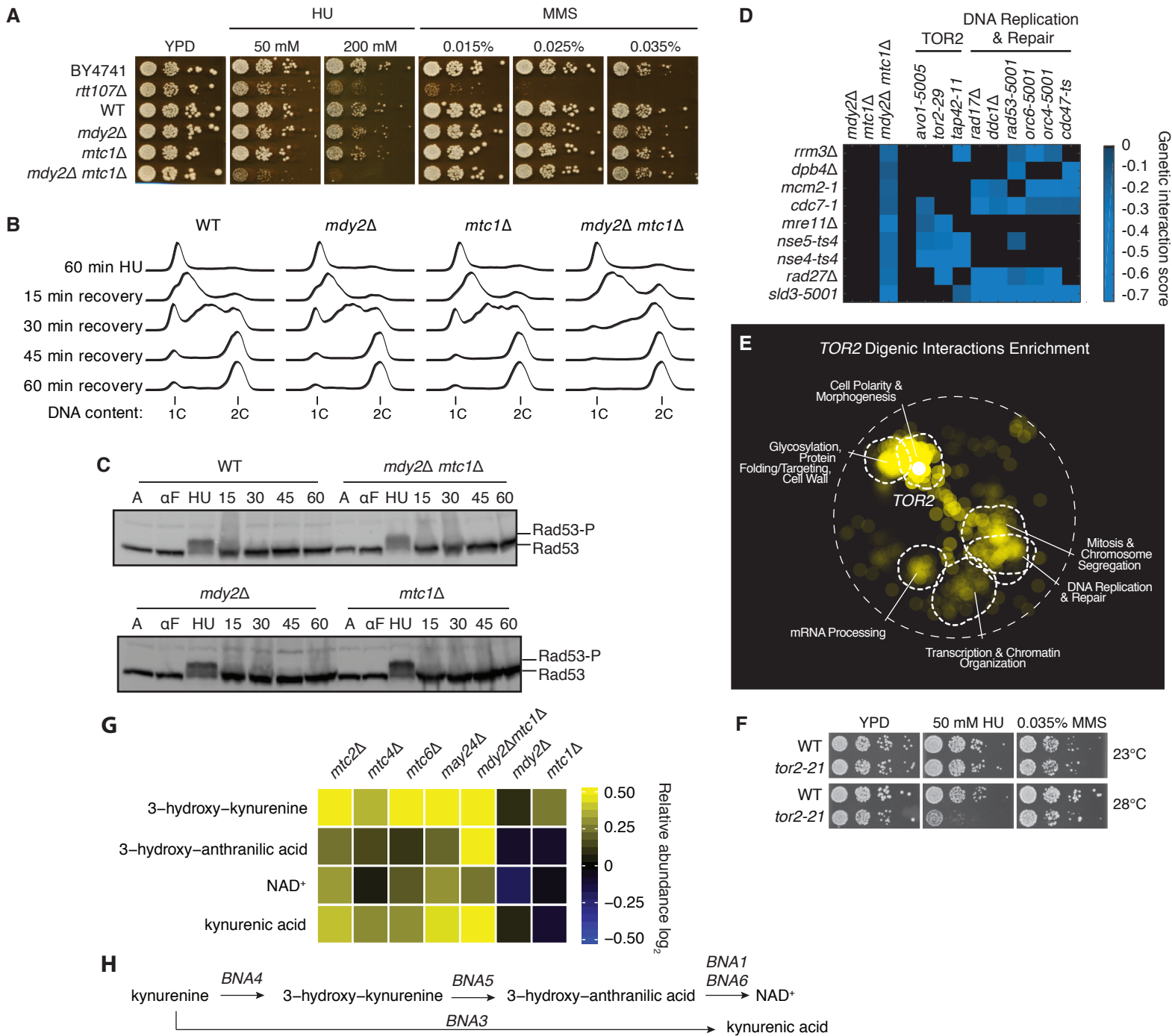


Fig. S10. DNA replication defect of *mdy2Δ mtc1Δ* double mutant. (A) The *mdy2Δ mtc1Δ* double mutant exhibits a DNA replication specific defect. Serial 10-fold dilutions of wild-type (BY4741, Y13096), *rtt107Δ*, *mdy2Δ*, *mtc1Δ* and *mdy2Δ mtc1Δ* cell cultures were spotted onto YPD and YPD + various concentrations of HU or MMS and incubated at 30°C for 3 days. The *rtt107Δ* mutant has a known fitness defect on media containing HU or MMS (70). (B) S-phase progression analysis following exposure to HU using flow cytometry. The *mdy2Δ mtc1Δ* double mutant exhibits more rapid progression through S phase than single mutants or wild-type after recovery of exposure to 100 mM HU. (C) The *mdy2Δ mtc1Δ* double mutant exhibits normal checkpoint activation and recovery during HU treatment. Western blot using extracts derived from the indicated strains and probed with an anti-Rad53 polyclonal antibody to detect Rad53 and phosphorylated Rad53. (D) *MDY2-MTC1* trigenic interactions derived from the DNA replication & repair bioprocess cluster in Fig. 4E are shown on the y-axis. Representative genes residing in biclusters derived from digenic interaction profiles that overlap with the *MDY2-MTC1* DNA replication & repair trigenic interactions are shown on the x-axis and involve genes with roles in DNA replication and repair and TOR2 signaling suggesting that the *mdy2Δ mtc1Δ* double mutant is partially defective for TOR2 function. (E) *MDY2-MTC1* trigenic interaction profile is similar to the TOR2 digenic profile. TOR2 digenic interactions from a composite profile of *tor2-21* and *tor2-29* showing bioprocess enrichments are highlighted. The query node depicts the average position lying equidistant from *tor2-21* and *tor2-29* nodes. (F) Growth response to HU and MMS for the *tor2-21* mutant resembles that of *mdy2Δ mtc1Δ* double mutant. These results are consistent with emerging evidence of a link between TOR2 and DNA replication and repair (73), although *MDY2-MTC1* double mutant query shows a relatively weak synthetic sick trigenic interaction with TOR1 suggesting of a partial, relatively weak, defect in Tor2 function. (G) The *mdy2Δ mtc1Δ* double mutant has elevated levels of metabolites involved in *de novo* biosynthesis of NAD⁺ from kynurenine which is involved in telomere uncapping (7,75,76) and possibly influences DNA synthesis pathways. Metabolite concentrations for kynurenine pathway intermediates for various deletion mutants. Values are normalized to ¹³C ¹⁵N internal standard for co-eluting peaks, normalized to a wild-type, and expressed on the log₂ scale. (H) Metabolic pathway for *de novo* biosynthesis of NAD⁺ from kynurenine.

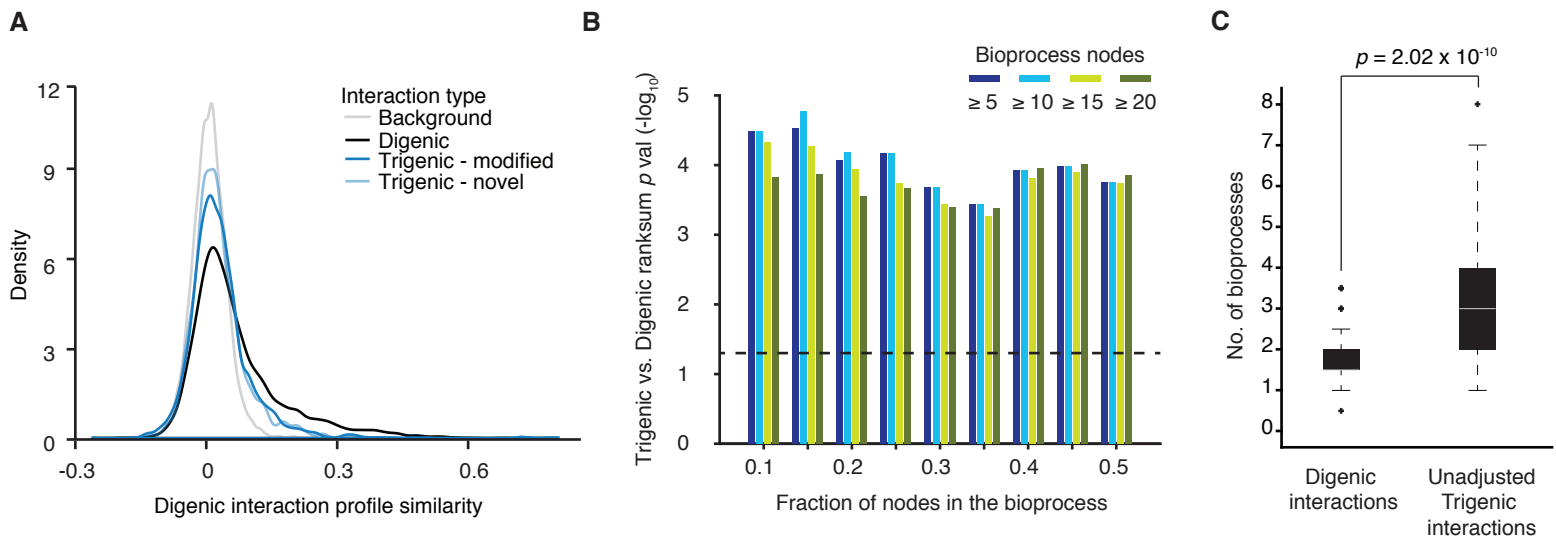
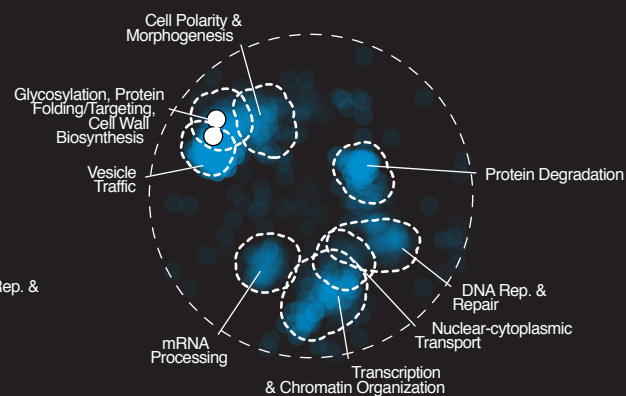
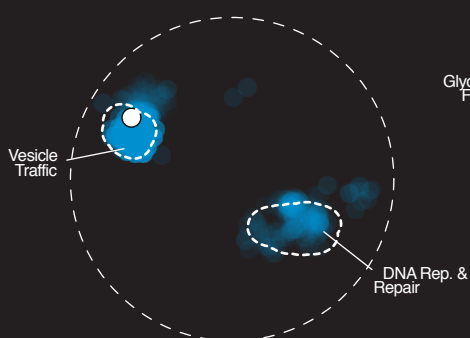
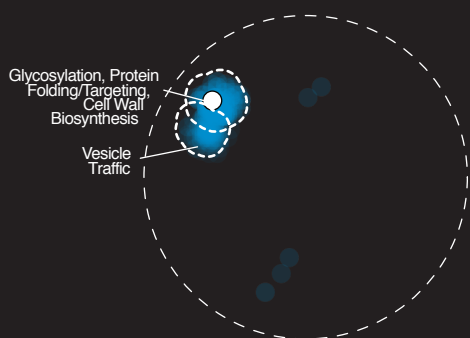
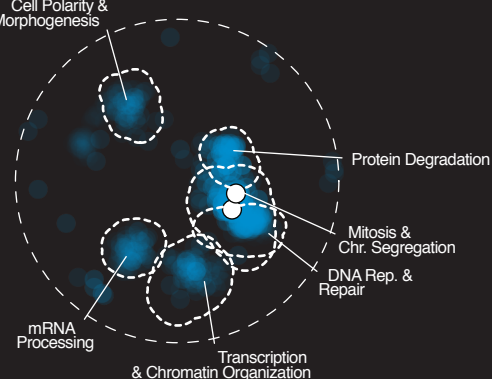
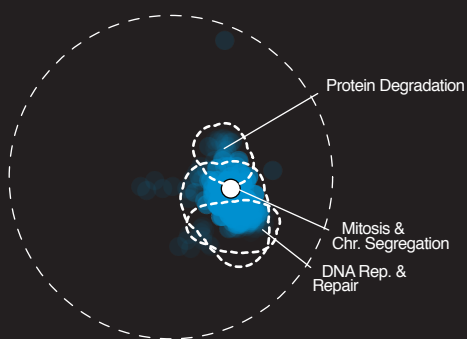
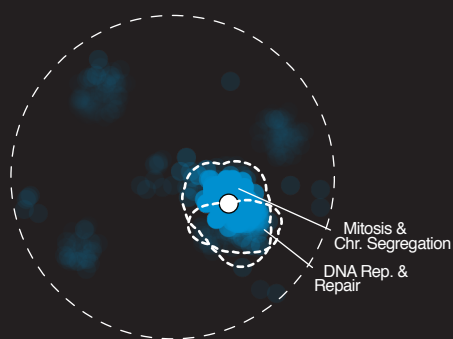
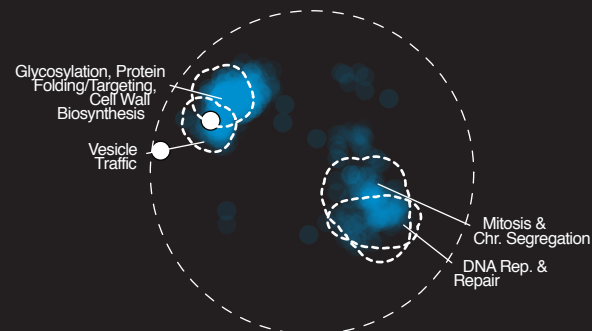
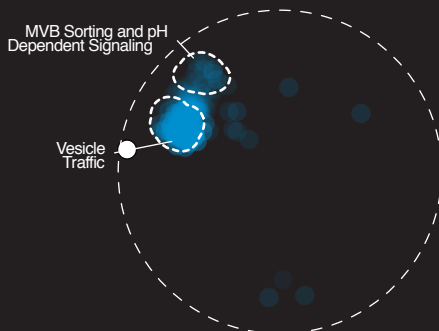
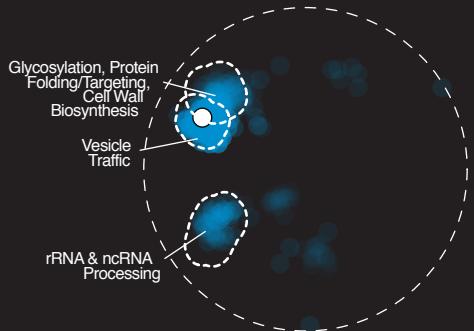
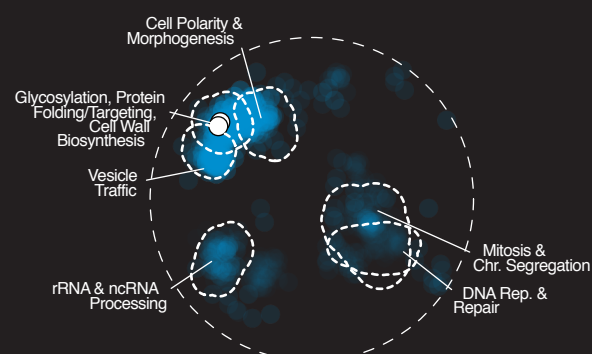
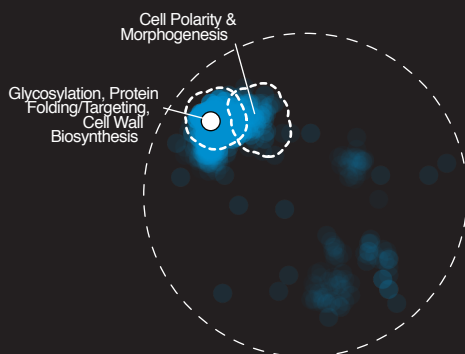
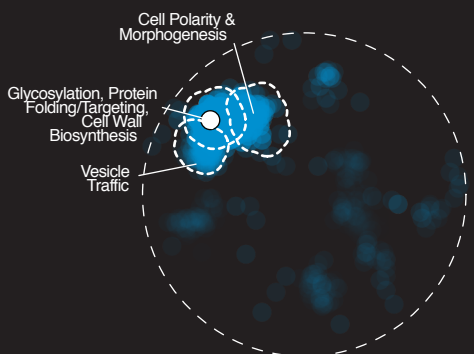


Fig. S11. Trigenic interactions are more functionally distant than digenic interactions. (A) Genetic Interaction profile similarity distributions of gene pairs involved in trigenic and digenic interactions in the entire data set corresponding to Fig. 6A. **(B)** The number of SAFE bioprocess clusters to which trigenic interactions map is higher than it is for digenic interactions, corresponding to Fig. 6C. **(C)** The number of SAFE bioprocess clusters enriched for unadjusted trigenic interactions, which is significantly different from digenic interactions (signed rank sum test $p = 2.02 \times 10^{-10}$) similar to the difference observed for adjusted trigenic interactions in Fig. 6C. **(D)** The digenic interaction similarity network was annotated using SAFE, identifying network regions enriched for similar GO biological process terms of representative query pairs trigenic and digenic interactions, which are outlined in dashed lines. Positions of the query genes are denoted with a white circle (see next page). Query genes that are connected to other genes with a Pearson correlation coefficient < 0.2 do not appear on the global similarity map, specifically *ERV29* and *PML39*, thus their query nodes represent the gene that they are most highly correlated with such as *spc3-4* and *nup57-5001*, respectively (7). Refer to (16) for details on measuring functional diversity.

D

Digenic Interactions

Trigenic Interactions

*ERV29**ERV25**ERV29 - ERV25**MAD2**SLK19**MAD2 - SLK19**MVP1**MRL1**MVP1 - MRL1**KRE1**ALG6**KRE1 - ALG6*

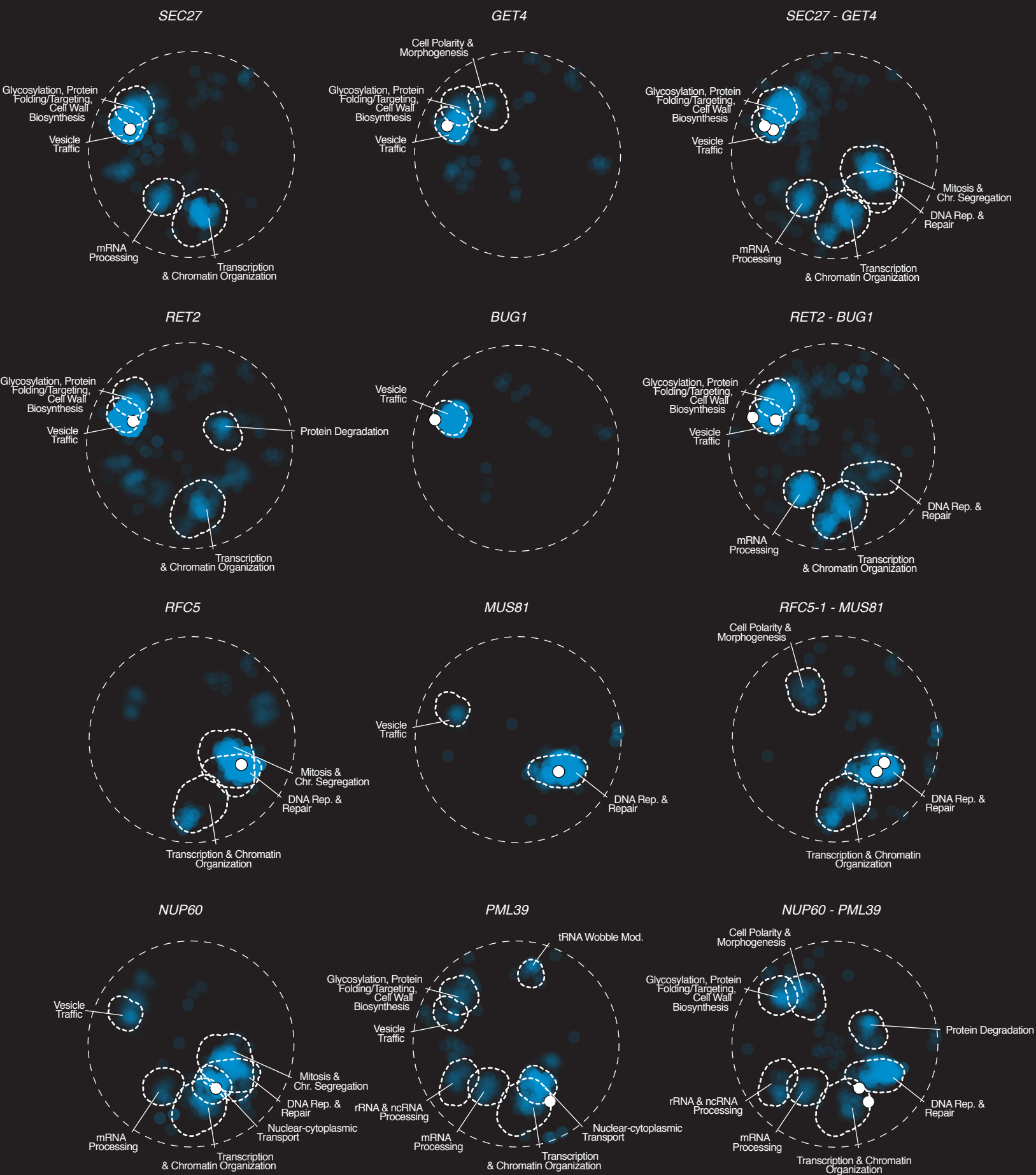
● Query gene

Fig. S11. (D) See legend on previous page.

D

Digenic Interactions

Trigenic Interactions



● Query gene

Fig. S11. (D) Continued from previous page.

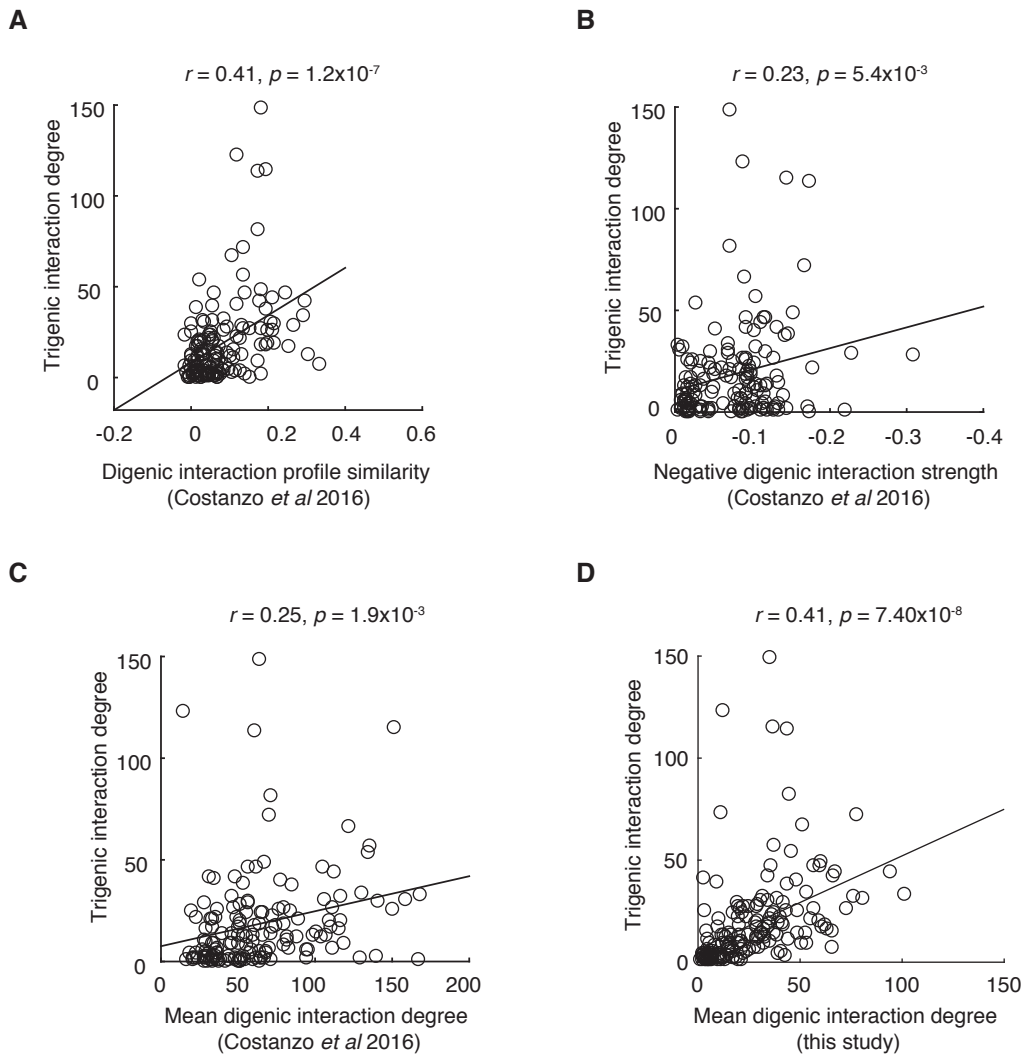


Fig. S12. Digenic interaction network features are predictive of trigenic degree. (A) Scatter plot of the correlation of trigenic interaction degree and average digenic interaction profile similarity, Pearson correlation coefficient, $r = 0.41, p = 1.2 \times 10^{-7}$. (B) Scatter plot of the correlation of trigenic interaction degree and digenic interaction strength, Pearson correlation coefficient, $r = 0.23, p = 5.4 \times 10^{-3}$. (C) Scatter plot of the correlation of trigenic interaction degree and digenic interaction degree, Pearson, $r = 0.25, p = 1.9 \times 10^{-3}$. (D) Scatter plot of the correlation of trigenic degree and digenic interaction degree, Pearson, $r = 0.41, p = 7.40 \times 10^{-8}$. Digenic network features for (Fig. S11A-C) were derived from a previous study (7) and are for the set of double mutants that was also used for conservative extrapolation results depicted in Fig. 7D, Fig. S13A and Additional Data S7. For (D) digenic interaction network features are from this study measured across all mutants that were screened. Genetic interaction degrees are for thresholds: τ or $\varepsilon < -0.08, p < 0.05$.

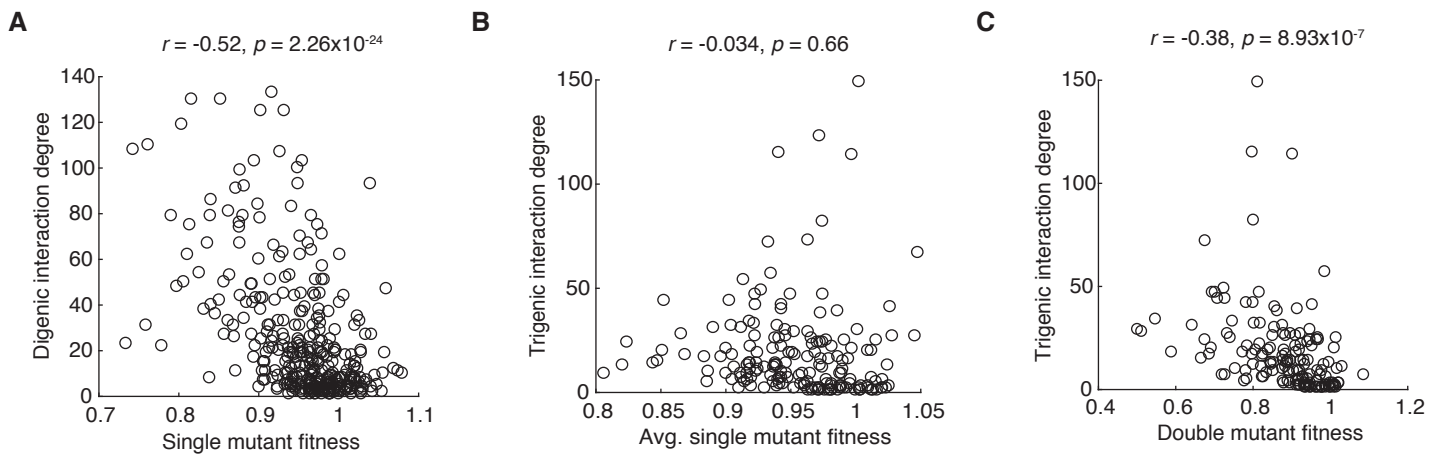
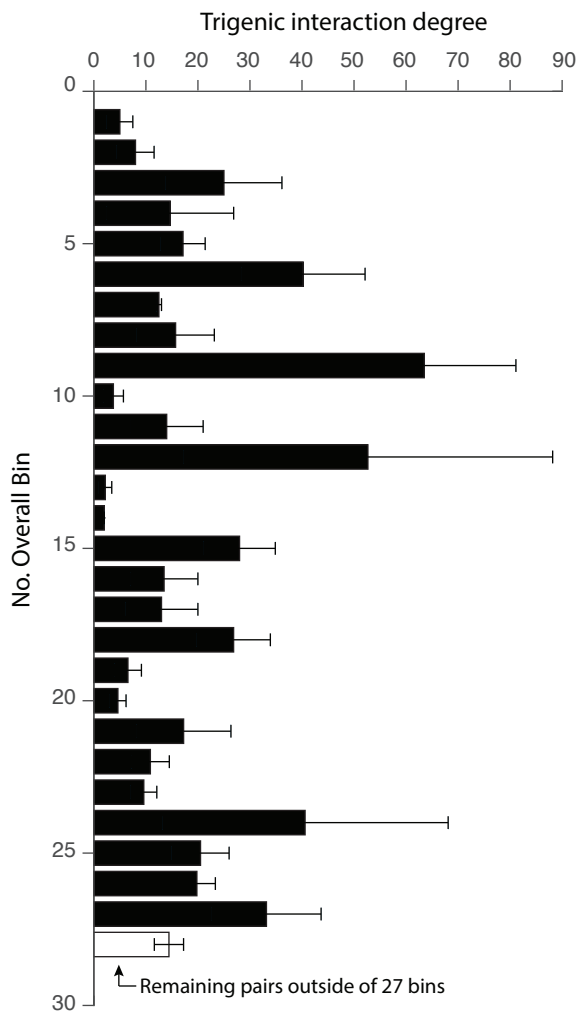


Fig. S13. Double mutant fitness correlates with trigenic interaction degree. (A) Scatter plot depicting the correlation between digenic interaction degree and single mutant fitness, Pearson correlation coefficient, $r = -0.52$, $p = 2.26 \times 10^{-24}$. (B) Scatter plot depicting the lack of a correlation between trigenic interaction degree and average single mutant fitness, Pearson correlation coefficient, $r = -0.034$, $p = 0.66$. (C) Scatter plot depicting the correlation between trigenic degree and double mutant fitness, Pearson correlation coefficient, $r = -0.38$, $p = 8.93 \times 10^{-7}$.



Overall bin no.	Neg. Digenic interaction score	Digenic interaction degree	Digenic interaction profile similarity
1	moderate	low	low
2	moderate	low	intermediate
3	moderate	low	high
4	moderate	intermediate	low
5	moderate	intermediate	intermediate
6	moderate	intermediate	high
7	moderate	high	low
8	moderate	high	intermediate
9	moderate	high	high
10	weak	low	low
11	weak	low	intermediate
12	weak	low	high
13	weak	intermediate	low
14	weak	intermediate	intermediate
15	weak	intermediate	high
16	weak	high	low
17	weak	high	intermediate
18	weak	high	high
19	zero - very weak	low	low
20	zero - very weak	low	intermediate
21	zero - very weak	low	high
22	zero - very weak	intermediate	low
23	zero - very weak	intermediate	intermediate
24	zero - very weak	intermediate	high
25	zero - very weak	high	low
26	zero - very weak	high	intermediate
27	zero - very weak	high	high

Fig. S14. Average trigenic interaction degree for query binned according to digenic interaction features used for extrapolation estimates. Mean trigenic interaction degree is shown, bars are SEM.

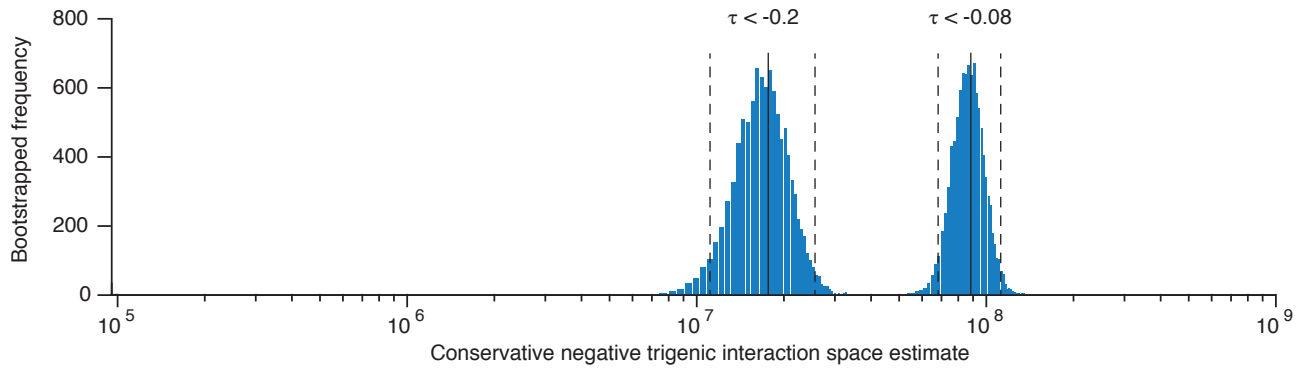
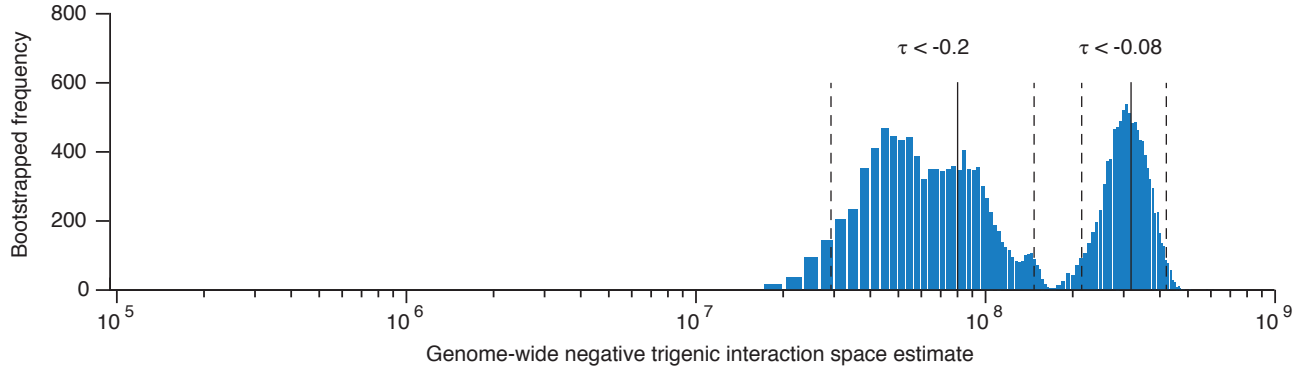
A**B**

Fig. S15. Estimate of the number of trigenic interactions. **(A)** Conservative estimates of the number of trigenic interactions at intermediate ($\tau < -0.08$) and very stringent cut-offs ($\tau < -0.2$) based on query strain assignment to their respective 27 bins based on digenic interaction network parameters: i) digenic interaction profile similarity (bin thresholds: -0.02, 0.03, 0.1, $+\infty$); ii) digenic interaction score between constitutive single mutants (bin thresholds: 0, -0.08, -0.1, $-\infty$); and iii) average digenic interaction degree of constitutive mutants (bin thresholds: 10, 45, 70, $+\infty$). **(B)** Genome-wide estimates at intermediate ($\tau < -0.08$) and very stringent cut-offs ($\tau < -0.2$). A fourth bin was added along the axes in Fig. 1A to accommodate potential double mutant queries with values missing or outside stated ranges: digenic profile similarity: $(-\infty, -0.02)$, digenic interaction strength: $(0, +\infty)$. Bootstrapping was used to generate the estimate by sampling with replacement 10,000 times, 95% C.I. is depicted by the dashed lines, the median estimate of the extent of trigenic interaction space is denoted with a solid black line. Refer to (16) for extrapolation details.

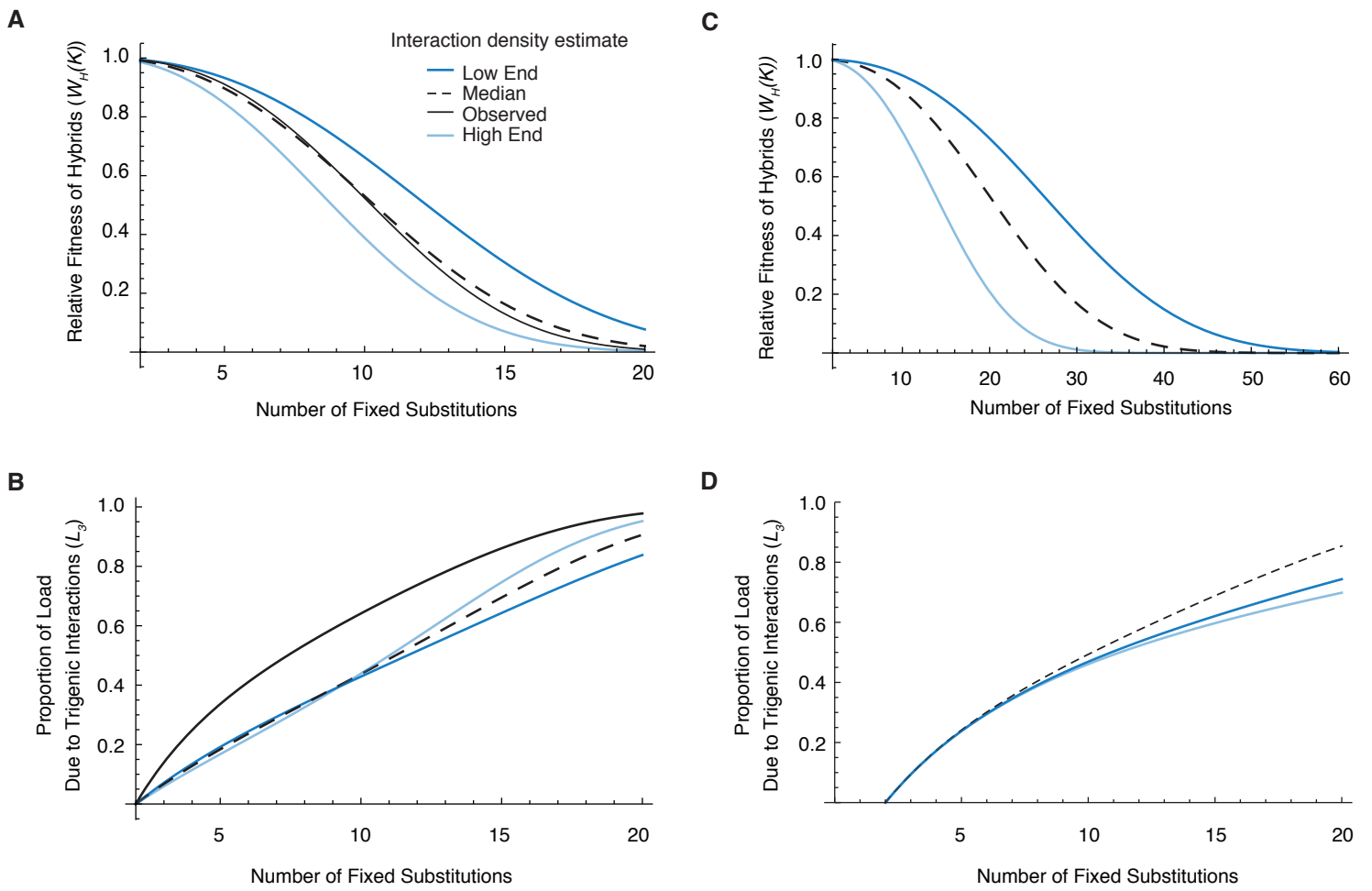


Fig. S16. 2-locus and 3-locus Dobzhansky-Muller Incompatibility Model for Speciation. **(A)** The expected relative hybrid fitness vs. the number of fixed differences between populations. The fitness of hybrids declines rapidly due to the strongly deleterious digenic and trigenic interactions measured in this study. Within 20 fixed loss-of-function mutations, we would expect hybrid fitness to drop drastically. For calculation of hybrid fitness refer to the equation for $W_H(K)$ in (16) section ‘Parametrizing Dobzhansky-Muller Incompatibility Models’, density parameters are from Table S4 and $\varepsilon_2 = -0.25$, $\varepsilon_3 = -0.186$. **(B)** The proportion of hybrid load (decrease in fitness of the hybrid compared to the parent populations) due to deleterious effects of trigenic interactions vs. the number of fixed differences between populations. While trigenic interactions are both rarer and weaker in effect, under all of the examined estimates of their rarity we find that they are expected to contribute the majority of hybrid load following just 10 substitutions. While the overall strength of interactions may be overestimated, these results suggest that trigenic interactions may play an important role in speciation. For calculation of proportion of hybrid load due to trigenic interactions refer to the equation for L_3 in (16) section ‘Parametrizing Dobzhansky-Muller Incompatibility Models’, density parameters are from Table S4 and $\varepsilon_2 = -0.25$, $\varepsilon_3 = -0.186$. **(C)** The expected relative hybrid fitness vs. the number of fixed differences between populations. If we extrapolate the relative frequency and strength of hybrid interactions and use them as parameters together with the measured density and strength of digenic interactions in the nearly complete network from Costanzo *et al.* (7), we find that hybrid fitness declines much more slowly compared to (A). Hybrid fitness was calculated using equation described in (A), low end $p_2 = -0.0015$, median $p_2 = -0.003$, high end $p_2 = -0.006$; $p_3 = 0.12(p_2)$. **(D)** The proportion of hybrid load (decrease in fitness of the hybrid compared to the parent populations) due to deleterious effects of trigenic interactions vs. the number of fixed differences between populations using parameters from extrapolated trigenic interaction frequency and global digenic interaction network described in (C). Trigenic interactions are expected to contribute the majority of hybrid load following just 15 substitutions, consistent with (B) supporting the notion that trigenic interactions may play an important role in speciation. For calculation of proportion of hybrid load due to trigenic interactions refer to the equation for L_3 in (16) section ‘Parametrizing Dobzhansky-Muller Incompatibility Models’.

Table S1. Selection criteria for query gene pairs for testing trigenic interaction space.

Boundary reflects the four thresholds chosen to generate three bins. Percentile reflects the proportion of gene-pairs found within the indicated thresholds. Digenic interaction score is the digenic interaction score between two query genes. Digenic interaction degree is the average number of digenic interactions of a given query gene pair. Digenic interaction profile similarity is represented by the Pearson correlation coefficient of the digenic interaction profiles of the two query genes. Total number of bins: $3^3 = 27$; mean number of query genes per bin = 5.6. All three digenic interaction parameters were derived from the global digenic interaction network (7). Refer to (16) for more details.

	Digenic interaction score				Digenic interaction degree				Digenic interaction profile similarity			
Boundary	$-\infty$	-0.1	-0.08	0	10	45	70	$+\infty$	-0.02	0.03	0.1	$+\infty$
Percentile	0	2.4	3.7	53	1.4	29	56	100	24	75	98	100
No. query	45	32	74		50	53	48		46	59	46	

Table S2. Validation of *cln1Δ cln2Δ* trigenic interactions by tetrad and random spore analyses (TA and RSA, respectively).

SS = synthetic sick, SL = synthetic lethal. Refer to (16) for validation details.

Gene name	ORF	τ	p-value	Confirm. test	Confirm. result
<i>APL6</i>	YGR261C	-0.25	6.55×10^{-3}	RSA	inconclusive
<i>APS3</i>	YJL024C	-0.13	1.11×10^{-2}	RSA	SS
<i>BEM2</i>	YER155C	-0.42	1.96×10^{-4}	TA	SL
<i>BUD2</i>	YKL092C	-0.69	1.60×10^{-9}	TA	SS/SL
<i>BUD6</i>	YLR319C	-0.30	1.75×10^{-2}	RSA	SS
<i>CLB5</i>	YPR120C	-0.45	1.48×10^{-2}	RSA	SS
<i>CLN3</i>	YAL040C	-0.61	5.34×10^{-10}	TA	SS/SL
<i>CSF1</i>	YLR087C	-0.21	7.03×10^{-4}	RSA	SS
<i>CYK3</i>	YDL117W	-0.20	3.81×10^{-6}	TA	SS/SL
<i>DBF2</i>	YGR092W	-0.62	1.51×10^{-6}	RSA	SS
<i>EAF7</i>	YNL136W	-0.20	3.57×10^{-2}	RSA	SS
<i>EDE1</i>	YBL047C	-0.20	4.91×10^{-2}	RSA	inconclusive
<i>FYV10</i>	YIL097W	-0.14	1.67×10^{-2}	RSA	SS
<i>GAS1</i>	YMR307W	-0.29	1.67×10^{-6}	RSA	SS
<i>GBP2</i>	YCL011C	-0.24	4.02×10^{-2}	RSA	SS
<i>GET2</i>	YER083C	-0.23	2.14×10^{-4}	TA	SL
<i>GUP1</i>	YGL084C	-0.27	4.33×10^{-2}	RSA	SS
<i>HSL1</i>	YKL101W	-0.56	9.57×10^{-10}	RSA	SS
<i>LGE1</i>	YPL055C	-0.32	2.72×10^{-4}	TA	SS
<i>LSM1</i>	YJL124C	-0.55	4.24×10^{-6}	TA	SS/SL
<i>LSM7</i>	YNL147W	-0.28	1.71×10^{-3}	RSA	not confirmed
<i>NBP2</i>	YDR162C	-0.38	1.08×10^{-2}	TA	inconclusive
<i>NUP188</i>	YML103C	-0.23	1.21×10^{-2}	RSA	SS
<i>PAT1</i>	YCR077C	-0.40	2.65×10^{-3}	RSA	inconclusive
<i>PEP8</i>	YJL053W	-0.38	3.66×10^{-4}	RSA	SS
<i>RTF1</i>	YGL244W	-0.24	1.33×10^{-2}	TA	SS
<i>RUD3</i>	YOR216C	-0.32	2.45×10^{-4}	RSA	SS
<i>RXT2</i>	YBR095C	-0.12	4.61×10^{-2}	RSA	inconclusive
<i>SAC7</i>	YDR389W	-0.50	4.70×10^{-6}	RSA	SS
<i>SAP190</i>	YKR028W	-0.17	4.91×10^{-2}	RSA	inconclusive
<i>SDC1</i>	YDR469W	-0.40	1.74×10^{-4}	RSA	SS
<i>SDS3</i>	YIL084C	-0.41	2.03×10^{-4}	RSA	inconclusive
<i>SMI1</i>	YGR229C	-0.37	7.92×10^{-4}	RSA	SS
<i>SNX4</i>	YJL036W	-0.25	1.15×10^{-2}	RSA	SS
<i>SRN2</i>	YLR119W	-0.38	7.84×10^{-6}	RSA	SS
<i>SWD1</i>	YAR003W	-0.25	1.88×10^{-2}	RSA	SS
<i>SWI4</i>	YER111C	-0.24	7.76×10^{-6}	TA	not confirmed
<i>TLG2</i>	YOL018C	-0.16	2.73×10^{-2}	RSA	SS
<i>VAC14</i>	YLR386W	-0.38	1.64×10^{-2}	RSA	inconclusive
<i>VAM6</i>	YDL077C	-0.49	8.21×10^{-5}	RSA	SS
<i>VAM7</i>	YGL212W	-0.38	1.55×10^{-2}	RSA	SS
<i>VPS29</i>	YHR012W	-0.32	3.21×10^{-2}	RSA	SS
<i>VPS35</i>	YJL154C	-0.48	7.55×10^{-6}	RSA	SS
<i>VPS60</i>	YDR486C	-0.29	1.94×10^{-2}	RSA	SS

Table S3. Comparison of the global digenic and trigenic interaction networks based on the set of screened query genes.

Extrapolated digenic (genome-wide) and trigenic (conservative) estimates are based on Fig. 7D, Fig. S15A; and extrapolated trigenic (genome-wide) estimates are based on Fig. S13B. Observed significant digenic and trigenic interactions are counted from single mutant control queries and double mutant queries, respectively, from this study. Extrapolated digenic interactions are derived from a larger digenic interaction survey (7), and incorporate estimates of false positive and false negative rates. Two extrapolations of negative trigenic interactions are provided, the first (conservative) covers a subset of the total space where more confident predictions can be made (Fig. 7D, S15A), while another, less confident prediction is provided for the entire genome (Fig. S15B). See (16) for extrapolation details. The number of digenic and trigenic interaction estimates are shown and the 95% confidence intervals are in brackets.

	Global Digenic Network		Global Trigenic Network			
	Observed (this study)	Extrapolated (genome-wide)	Observed (this study)	Extrapolated (conservative)	Observed (this study)	Extrapolated (genome-wide)
Queries	302 (subset)	-	151(subset)	-	182 (all)	-
Arrays	1,182	-	1,182	-	1,182	-
Negative Interactions (95% C.I.)	7,660	6.28×10^5 (4.0×10^5 – 9.8×10^5)	2,792	8.99×10^7 (6.9×10^7 - 1.1×10^8)	3,196	3.24×10^8 (2.2×10^8 – 4.3×10^8)
No. total possible mutants	324,717 pairs	~ 18 million pairs	162,270 triads	~ 9.4 billion triads (26% of all triads)	195,666	~ 36 billion triads (all possible triads)
Interaction frequency (95% C.I.)	2.25%	3.59% (2.27 – 5.62%)	1.72%	1.10% (0.84 - 1.4%)	1.63%	1.03% (0.70 - 1.37%)

Table S4: Estimates of the density of digenic/trigenic interactions under various scenarios, used to calculate the expected rate of speciation.

‘Median’ density estimate refers to the estimated significant negative genetic interaction density based on the global digenic interaction network (7) and the estimated genome-wide trigenic interaction density is depicted in Table S3. ‘Low end’ and ‘high end’ refer to digenic and trigenic density estimates from Table S3 and reflect the false positive and false negative rates, respectively, associated with SGA genetic interaction screens.

‘Directly observed’ density estimates refer to the estimated significant negative genetic interaction densities that were directly observed in this study from screening the entire set of 182 double mutant and 364 single mutant query strains. Refer to (16) for extrapolation details.

Estimate	Digenic interaction density (α_2)	Trigenic interaction density (α_3)
Low end	0.0227	0.0070
Median	0.0359	0.0103
High end	0.0562	0.0140
Directly observed	0.0251	0.0163

Table S5. Minimal genome size after accounting for digenic interactions.

For each fitness defect threshold, the total size of the minimal genome after accounting for digenic interactions is indicated. The essential gene set of 1,128 genes is included in the minimal genome for all settings of the “Minimum allowable fitness” parameter. See (16) for a summary of the algorithm used to perform this estimation.

Minimum allowable fitness	Minimal genome size (incl. 1128 essential genes)
0.1	1414
0.2	1719
0.3	1926
0.4	2145
0.5	2373
0.6	2635
0.7	3017
0.8	3539
0.9	4183

Additional Data S1. Raw genetic interaction dataset.

This file contains digenic interaction scores as well as raw and adjusted trigenic interaction scores in a tab-delimited format with 12 columns: 1) Query Strain ID, 2) Query allele name, 3) Array strain ID, 4) Array allele name, 5) Combined mutant type, 6) Raw genetic interaction score (epsilon), 7) Adjusted trigenic interaction score (tau), 8) p-value, 9) Query fitness, 10) Array single mutant fitness, 11) Combined mutant fitness relative to wild-type, 12) Combined mutant fitness standard deviation

Column description for each of the new supplemental files

1. Query Strain ID
2. Query Allele name
3. Array Strain ID
4. Array Allele name
5. Combined mutant type
 - a. 'digenic' for double mutants resulting from a cross between a single mutant control query and a single mutant array strain
 - b. 'trigenic' for triple mutants resulting from a cross between a double mutant query and a single mutant array strain
6. Raw genetic interaction score (epsilon)
7. Final genetic interaction score (trigenic tau / digenic epsilon). Trigenic scores are adjusted according to the τ -SGA model shown in Fig. S4A. Digenic scores receive no further adjustment and the epsilon value is repeated.
8. Interaction p value
9. Query fitness
 - a. single mutant fitness for single mutant queries
 - b. double mutant fitness for double mutant queries
10. Array single mutant fitness
11. Combined mutant fitness relative to wild-type.
 - a. Double mutant fitness for the resulting combined digenic mutants
 - b. Triple mutant fitness for the resulting combined trigenic mutants
12. Combined mutant fitness standard deviation

Additional Data S2. Digenic and adjusted trigenic interaction dataset.

This file contains digenic and trigenic interaction scores at an established interaction magnitude cut-off for digenic interactions ($p < 0.05$, $|\epsilon| > 0.08$) and trigenic interactions ($p < 0.05$, $\tau < -0.08$) in a tab-delimited format with 8 columns: 1) Query Strain ID, 2) Query allele name, 3) Array strain ID, 4) Array allele name, 5) Combined mutant type, 6) Final genetic interaction score (tau), 7) p-value, 8) Interaction type

Column description for each of the new supplemental files

1. Query Strain ID
2. Query Allele name
3. Array Strain ID
4. Array Allele name

5. Combined mutant type
 - a. ‘digenic’ for double mutants resulting from a cross between a single mutant control query and a single mutant array strain
 - b. ‘trigenic’ for triple mutants resulting from a cross between a double mutant query and a single mutant array strain
6. Final genetic interaction score (trigenic tau / digenic epsilon). Trigenic scores are adjusted according to the τ -SGA model shown in Fig. S4A and account for any digenic interactions. Digenic scores receive no further adjustment and the epsilon value is repeated from Additional Table S1.
7. Interaction *p* value
8. Interaction types:
 - a. **Digenic** is digenic
 - b. **Novel** is novel trigenic
 - c. **Unclassified** apparently novel but with unknown query-query interaction score thus cannot be distinguished from modified and novel
 - d. **Modified Q-**, **Modified Q-A-**, **Modified Q-A+**, **Modified Q-A+-**, **Modified A-**, **Modified A+** or **Modified A+-** are modified trigenic interactions are further broken down by where the overlapping digenic interaction is found: Q- for a negative interaction between query genes, A- for a negative interaction between one or both of the query genes and the array gene, A+ for a positive interaction between one or both of the query genes and the array gene, A+- if both query genes have a digenic interaction with the array but of opposing signs)

Additional Data S3. Query strains and plasmids list.

This file contains the complete list of yeast strains and plasmids that were used in this study. The ‘Strain Pairing List’ tab lists the double mutants and their corresponding single mutant control strains that were used to generate trigenic interaction scores. The ‘Genotypes’ tab lists the complete genotype of each strain including control strains that were used to derive the fitness standard. The ‘Plasmids’ tab lists that plasmids that were used in this study.

Additional Data S4. Fitness standard for single and double mutant query strains.

This file contains the fitness standard for single and double mutant query strains.

Additional Data S5. Diagnostic array strain list.

This file contains the complete list of yeast strains present on the diagnostic array, which was used for genetic interaction screens in this study.

Additional Data S6. *MDY2-MTC1* genetic interaction list.

This file contains the trigenic interactions list of *MDY2-MTC1* and digenic interaction list of *MDY2* and *MTC1* corresponding to Fig. 3. The ‘Tetrad Analysis’ tab contains confirmations results obtained from tetrad analysis: SS is synthetic sick, SL is synthetic lethal. The ‘Genetic interactions’ tab contains columns that are annotated with ‘CellMap’ since they contain genetic interactions from (7) downloaded from theCellMap.org (27) as well as scores derived in this study.

Additional Data S7. Query bins for trigenic interaction space extrapolation.

This file contains a list of queries used for trigenic interaction space extrapolation. The digenic interaction parameters used for binning for each double mutant query and its single mutant counterparts was derived from the global digenic interaction network (7).

1. Gene1 - gene2 double mutant query strain ID
2. Gene1 single mutant control query strain ID
3. Gene2 single mutant control query strain ID
4. ORF1
 - a. associated with gene1 single mutant control query strain and gene1 of the double mutant query strain
5. ORF2
 - a. associated with gene2 single mutant control query strain and gene2 of the double mutant query strain
6. Gene1
7. Gene2
8. Allele1
 - a. associated with gene1 single mutant control query strain and gene1 of the double mutant query strain
9. Allele2
 - a. associated with gene2 single mutant control query strain and gene2 of the double mutant query strain
10. DigenicInteractionScore
 - a. digenic interaction score between constitutive single mutants
11. DigenicInteractionScore_bin
 - a. Bin assignments for digenic interaction score: 1) $\epsilon < -0.1$; 2) $-0.1 \leq \epsilon < -0.08$; 3) $-0.08 \leq \epsilon < 0$
12. DigenicInteractionScore_bin_name
 - a. Name for bin assignments for digenic interaction score: 1) moderately negative digenic interaction score; 2) weakly negative digenic interaction score; 3) very weakly negative digenic interaction score
13. DigenicDegree
 - a. average digenic interaction degree of constitutive mutants
14. DigenicDegree_bin
 - a. Bin assignments for digenic degree: 1) $10 \leq \text{degree} < 45$; 2) $45 \leq \text{degree} < 70$; 3) $70 \leq \text{degree}$
15. DigenicDegree_bin_name
 - a. Name for bin assignments for digenic interaction degree: 1) low avg. digenic interaction degree; 2) intermediate avg. digenic interaction degree; 3) high avg. digenic interaction degree
16. AvgProfileSimilarity
 - a. average digenic interaction profile similarity for constitutive single mutants
17. AvgProfileSimilarity_bin
 - a. Bin assignments for average digenic interaction profile similarity (r): 1) $-0.02 < r < 0.03$; 2) $0.03 \leq r < 0.1$; 3) $0.1 \leq r$
18. AvgProfileSimilarity_bin_name

- a. Name for bin assignments for average digenic interaction profile similarity: 1) low profile similarity; 2) intermediate profile similarity; 3) high profile similarity

19. TrigenicDegree

- a. Number of trigenic interactions per double mutant

20. OverallBin

- a. The bin number to which a specified query double mutant was assigned